University of Maribor
Faculty of Energy Technology

Journal of ENERGY TECHNOLOGY

Volume 8 / Issue 2
OCTOBER 2015
www.fe.um.si/en/jet.html

Journal of ENERGY TECHNOLOGY

VOLUME 8 / Issue 2

Revija Journal of Energy Technology (JET) je indeksirana v bazI INSPEC©.
The Journal of Energy Technology (JET) is indexed and abstracted in database INSPEC©.

JOURNAL OF ENERGY TECHNOLOGY

Izhajanje revije / PUBLISHING
Revija izhaja štirikrat letno v nakladi 150 izvodov. Članki so dostopni na spletni strani revije - www.fe.um.si/si/jet.html / The journal is published four times a year. Articles are available at the journal's home page - www.fe.um.si/en/jet.html.
Cena posameznega izvoda revije (brez DDV) / Price per issue (VAT not included in price): 50,00 EUR
Informacije o naročninah / Subscription information: http://www.fe.um.si/en/jet/subscriptions.html

Lektoriranje / LANGUAGE EDITING
Terry T. JACKSON

Oblikovanje in tisk / DESIGN AND PRINT
Fotografika, Boštjan Colarič s.p.

Naslovna fotografija / COVER PHOTOGRAPH
Jurij AVSEC

Oblikovanje znaka revije / JOURNAL AND LOGO DESIGN
Andrej PREDIN

Ustanovni urednik / FOUNDING EDITOR
Andrej PREDIN

Izdajanje revije JET finančno podpira Javna agencija za raziskovalno dejavnost Republike Slovenije iz sredstev državnega proračuna iz naslova razpisa za sofinanciranje domačih znanstvenih periodičnih publikacij / The Journal of Energy Technology is co-financed by the Slovenian Research Agency.

Spoštovani bralci revije Journal of energy technology (JET)

Učinkovita raba energije in razvoj energetskih tehnologij so gonilo človeškega razvoja. Danes predstavlja energetika, poleg proizvodnje hrane in zdravja ljudi, enega najpomembnejših poslovnih stebrov. Žal se ideja znanstvenika Nikole Tesle o energiji, ki bi bila zastonj, do sedaj še ni uresničila. Gospodarski razvoj v svetu tudi v tem desetletju sloni na pretežni izrabi fosilnih virov, kar pa žal posledično povzroča ekološke probleme. Upajmo, da se bodo v Parizu predstavniki držav dogovorili o omejitvah izpusta toplogrednih plinov. Prihodnost energetike je prav gotovo v izdatnejši izrabi obnovljivih virov v povezavi z alternativno energetiko. O tem pišejo tudi nekateri avtorji člankov v tem in prejšnjih izvodih revije JET.

Jurij AVSEC
odgovorni urednik revije JET

Dear Readers of the Journal of Energy Technology (JET)

Efficient use of energy and development of new energy technologies is the driving force of human development. Today, energy technology is one of the most important pillars of business, in addition to food production and human health. Unfortunately, the idea of the scientist Nikola Tesla that energy would be free has not materialized thus far. The economic development in this decade in the world is still based on the dominant exploitation of fossil resources, which unfortunately has led to some ecological problems. Currently, Paris will be occupied by representatives of almost all nations; hopefully restrictions on the greenhouse gas emissions will be agreed on. The future is undoubtedly in the increase of exploitation of renewable energy sources. Several articles in this and previous issues of JET discuss this.

Jurij AVSEC
Editor-in-chief of JET

Table of Contents / Kazalo

JET Journal of Energy Technology

JET Volume 8 (2015) p.p. 11-16
Issue 2, October 2015
Typology of article 1.01
www.fe.um.si/en/jet.html

DETERMINATION OF THE CONDITIONS FOR THE EXISTENCE OF HIGHER-ORDER DIFFERENTIAL ELECTROMAGNETIC INVARIANTS

DOLOČITEV POGOJEV ZA OBSTOJ DIFERENCIALNIH ELEKTROMAGNETNIH INVARIANT VIŠJEGA REDA

Boris Nevzlin[1], Valentina Zagirnyak[✉], Veronika Zahorulko[2]

Keywords: four-element dipole, electromagnetic invariants, differential transformations, conditions for the existence of higher-order invariants

Abstract

A four-element dipole representation by first-order electromagnetic invariants according to differential transformation and increments is well known. The paper deals with a most general description of the conditions of existence of an electromagnetic invariant for a four-element dipole with active-reactive components in a differential form and as increments of any order. It is shown analytically that invariants exist at mutual transformations of increments into differentials and differentials into increments.

✉ Corresponding author: Valentina Zagirnyak, (Eng.), Tel.: +38 05366 36218, Fax: +38 05366 36000, Mailing address: Kremenchuk Mykhailo Ostrohradskyi National University, Manufacturing Engineering Department, Vul. Pershotravneva, 20, 39600, Kremenchuk, Ukraine, E-mail address: mzagirn@kdu.edu.ua

[1] Kremenchuk Mykhailo Ostrohradskyi National University, Electric machines and Apparatus Department, Vul. Pershotravneva, 20, 39600, Kremenchuk, Ukraine

[2] Kremenchuk Mykhailo Ostrohradskyi National University Electric machines and Apparatus Department, Vul. Pershotravneva, 20, 39600, Kremenchuk, Ukraine

Povzetek

Predstavitev dipola, sestavljenega iz štirih elementov, z elektromagnetno invarianto prvega reda je z vidika diferencialne transformacije in inkrementov že dobro poznana. Članek obravnava splošen opis pogojev za obstoj elektromagnetnih invariant dipola, sestavljenega iz štirih elementov, z delovno in jalovo komponento v diferencialni obliki in kot inkrementi poljubnega reda. Analitično je dokazano, da pri medsebojni transformaciji inkrementov v diference in diferenc v inkremente invariante obstajajo.

1 INTRODUCTION

A four-element dipole with active-reactive components (Fig. 1, a, b, c) is known [1, 2] to represent electromagnetic invariants according to differential transformation and increments that are of the form:

$$\frac{\frac{\partial C}{\partial \omega}}{\frac{\partial g}{\partial \omega}} = \frac{\partial C}{\partial g} = -\frac{C_1 + C_2}{g_1 + g_2}, \quad \frac{\frac{C_2 - C_1}{\omega_2 - \omega_1}}{\frac{g_2 - g_1}{\omega_2 - \omega_1}} = \frac{\Delta C}{\Delta g} = -\frac{C_1 + C_2}{g_1 + g_2}; \quad \frac{\frac{\partial \alpha}{\partial \omega}}{\frac{\partial R}{\partial \omega}} = \frac{\partial \alpha}{\partial R} = -\frac{\alpha_1 + \alpha_2}{R_1 + R_2},$$

$$\frac{\frac{\alpha_2 - \alpha_1}{\omega_2 - \omega_1}}{\frac{R_2 - R_1}{\omega_2 - \omega_1}} = \frac{\Delta \alpha}{\Delta R} = -\frac{\alpha_1 + \alpha_2}{R_1 + R_2}; \quad \frac{\frac{\partial L}{\partial \omega}}{\frac{\partial R}{\partial \omega}} = \frac{\partial L}{\partial R} = -\frac{L_1 + L_2}{R_1 + R_2}, \quad \frac{\frac{L_2 - L_1}{\omega_2 - \omega_1}}{\frac{R_2 - R_1}{\omega_2 - \omega_1}} = \frac{\Delta L}{\Delta R} = -\frac{L_1 + L_2}{R_1 + R_2}, \tag{1}$$

where ω –arbitrary circular frequency; ω_2, ω_1 –circular frequencies and $\omega_2 > \omega_1$; $C_2, \alpha_2, L_2, g_2, R_2$ –values C, α, L, g, R at frequency ω_2; $C_1, \alpha_1, L_1, g_1, R_1$ –values C, α, L, g, R at frequency ω_1.

Conditions for invariants existence consist of, respectively:

$$C_1 g_2 - C_2 g_1 \neq 0, \ \alpha_1 R_2 - \alpha_2 R_1 \neq 0, \ L_1 R_2 - L_2 R_1 \neq 0. \tag{2}$$

The same papers [1, 2] state that (1) there exist invariants not only according to frequency ω, but also according to order *n* of derivatives and increments:

$$\frac{\partial^n \tilde{N}}{\partial^n g} = \frac{\partial \tilde{N}}{\partial g} = -\frac{\tilde{N}_1 + \tilde{N}_2}{g_1 + g_2}, \quad \frac{\partial^n \alpha}{\partial^n R} = \frac{\partial \alpha}{\partial R} = -\frac{\alpha_1 + \alpha_2}{R_1 + R_2}, \quad \frac{\partial^n L}{\partial^n R} = \frac{\partial L}{\partial R} = -\frac{L_1 + L_2}{R_1 + R_2}, \tag{3}$$

but conditions for their existence are not given.

The purpose of this paper: determination of conditions for the existence of higher order invariants.

2 MATERIAL AND RESULTS OF RESEARCH

Second derivatives with respect to *C* and *g*:

$$\frac{\partial^2 \tilde{N}}{\partial \omega^2} = \frac{-2(C_1 + C_2)(C_1 g_2 - C_2 g_1)^2 \left[(g_1 + g_2)^2 - 3\omega^2 (C_1 + C_2)^2 \right]}{\left[(g_1 + g_2)^2 + \omega^2 (C_1 + C_2)^2 \right]^3},$$

$$\frac{\partial^2 g}{\partial \omega^2} = \frac{2(g_1+g_2)(C_1g_2 - C_2g_1)^2\left[(g_1+g_2)^2 - 3\omega^2(C_1+C_2)^2\right]}{\left[(g_1+g_2)^2 + \omega^2(C_1+C_2)^2\right]^3}. \quad (4)$$

The second condition for the existence of a second-order differential invariant follows from (4):

$$g_1 + g_2 \neq \sqrt{3}\omega(C_1 + C_2), \quad (5)$$

which is supplementary to (2).

Analogously, for a third-order differential invariant, the second condition for existence (the first one, as before, is (2)) is of the form:

$$g_1 + g_2 \neq \omega(C_1 + C_2), \quad (6)$$

and for the fourth one:

$$(g_1+g_2)^4 - 5\omega^2(C_1+C_2)^2\left[2(g_1+g_2)^2 - \omega^2(C_1+C_2)^2\right] \neq 0. \quad (7)$$

Condition (7), obviously, always exists at

$$\sqrt{2}(g_1+g_2) = \omega(C_1+C_2). \quad (8)$$

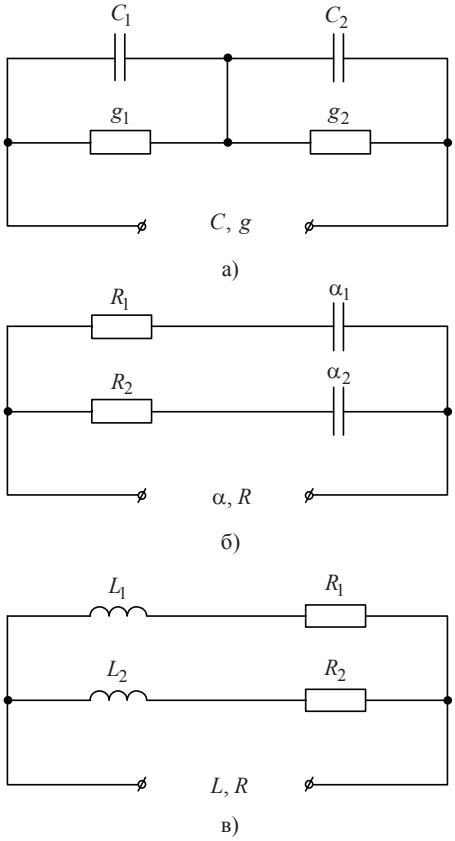

Figure 1: *Circuits of four-element dipoles: a) C_1, C_2 and C – condensers capacities and terminal capacitance of the circuit at arbitrary frequency, g_1, g_2 and g – the same concerning conductivity; b) α_1, α_2 and α – potential coefficients of condensers and overall potential*

coefficient of the circuit, R_1, R_2 and R – the same concerning resistances;
c) L_1, L_2, and L –branches inductances and overall inductance of the circuit,
R_1, R_2, and R – the same concerning resistances

Let us determine a derivative of the (*n*+1)-th order by a mathematical induction method, [3], in accordance with which a formula is considered true for any transformation, if it is proved that it, being true for *n*-th transformation, is also true for (*n*+1)-th transformation.
As invariant of the *n*-th order is of the form:

$$\frac{\partial^n \tilde{N}}{\partial^n g} = \frac{\dfrac{\partial^n \tilde{N}}{\partial \omega^n}}{\dfrac{\partial^n g}{\partial \omega^n}} = \frac{-\dfrac{\left(\tilde{N}_1+\tilde{N}_2\right)\left(\tilde{N}_1+\tilde{N}_2\right)^2\left(\tilde{N}_1 g_2-\tilde{N}_2 g_1\right)^2 f_n\left(C_1, C_2, g_1, g_2, \omega\right)}{\left[\left(g_1+g_2\right)^2+\omega^2\left(\tilde{N}_1+\tilde{N}_2\right)^2\right]^{n+1}}}{\dfrac{\left(g_1+g_2\right)\left(\tilde{N}_1+\tilde{N}_2\right)^2\left(\tilde{N}_1 g_2-\tilde{N}_2 g_1\right)^2 f_n\left(C_1, C_2, g_1, g_2, \omega\right)}{\left[\left(g_1+g_2\right)^2+\omega^2\left(\tilde{N}_1+\tilde{N}_2\right)^2\right]^{n+1}}}, \tag{9}$$

where $f_n\left(C_1, C_2, g_1, g_2, \omega\right)$ –the determined function for the derivative of the *n*-th order, e.g. for $n=3$ $f_n = -24\omega\left[\left(g_1+g_2\right)^2-\omega^2\left(C_1+C_2\right)^2\right]$.

Invariant of the (*n*+1)-th order is obtained:

$$\frac{\partial^{n+1} \tilde{N}}{\partial^{n+1} g} = \frac{\dfrac{\partial^{n+1} \tilde{N}}{\partial \omega^{n+1}}}{\dfrac{\partial^{n+1} g}{\partial \omega^{n+1}}} = \frac{-\dfrac{\left(\tilde{N}_1+\tilde{N}_2\right)\left(\tilde{N}_1+\tilde{N}_2\right)^2\left(\tilde{N}_1 g_2-\tilde{N}_2 g_1\right)^2\left\{\left[\left(g_1+g_2\right)^2+\omega^2\left(\tilde{N}_1+\tilde{N}_2\right)^2\right]\times\right.}{\left[\left(g_1+g_2\right)^2+\omega^2\left(\tilde{N}_1+\tilde{N}_2\right)^2\right]^{n+2}}\rightarrow}{\dfrac{\left(g_1+g_2\right)\left(\tilde{N}_1+\tilde{N}_2\right)^2\left(\tilde{N}_1 g_2-\tilde{N}_2 g_1\right)^2\left\{\left[\left(g_1+g_2\right)^2+\omega^2\left(\tilde{N}_1+\tilde{N}_2\right)^2\right]\times\right.}{\left[\left(g_1+g_2\right)^2+\omega^2\left(\tilde{N}_1+\tilde{N}_2\right)^2\right]^{n+2}}\rightarrow}$$

$$\rightarrow \frac{\left.\times\left\{\left[\left(g_1+g_2\right)^2+\omega^2\left(\tilde{N}_1+\tilde{N}_2\right)^2\right]\dfrac{\partial}{\partial\omega}\left[fn\left(C_1, C_2, g_1, g_2, \omega\right)\right]-\right.}{\left.\times\left\{\left[\left(g_1+g_2\right)^2+\omega^2\left(\tilde{N}_1+\tilde{N}_2\right)^2\right]\dfrac{\partial}{\partial\omega}\left[fn\left(C_1, C_2, g_1, g_2, \omega\right)\right]-\right.}\rightarrow$$

$$\rightarrow \frac{-2\omega(n+1)\left(\tilde{N}_1+\tilde{N}_2\right)^2 f_n\left(C_1, C_2, g_1, g_2, \omega\right)\}}{-2\omega(n+1)\left(\tilde{N}_1+\tilde{N}_2\right)^2 f_n\left(C_1, C_2, g_1, g_2, \omega\right)\}} = -\frac{\tilde{N}_1+\tilde{N}_2}{g_1+g_2}. \tag{10}$$

In this case, the condition for existence of (*n*+1)-th invariant, except (2), is of the form:

$$\left[\left(g_1+g_2\right)^2+\omega^2\left(\tilde{N}_1+\tilde{N}_2\right)^2\right]\frac{\partial}{\partial\omega}\left[f_n\left(C_1, C_2, g_1, g_2, \omega\right)\right] \neq$$
$$\neq 2(n+1)\omega\left(\tilde{N}_1+\tilde{N}_2\right)^2 f_n\left(C_1, C_2, g_1, g_2, \omega\right). \tag{11}$$

Thus, it can be stated that as a relation of any order derivatives of *C* and *g* with respect to frequency represents an invariant with respect to frequency, it is also an invariant with respect to the order of differential transformation with the condition for existence (2) for all invariants and (5) or (**6**), or (7)–(8) – for invariants of the determined orders (in a general form (**11**)).

Analogously to the circuits shown in Fig. 1, b, c, higher-order invariants are of the form (3) and, accordingly, conditions for their existence are of the form (except (2):

$$\omega\left(R_1+R_2\right)\neq\sqrt{3}\left(\alpha_1+\alpha_2\right), \tag{12}$$

$R_1+R_2\neq\sqrt{3}\omega\left(L_1+L_2\right)$ – second-order invariant,

$$\omega\left(R_1+R_2\right)\neq\alpha_1+\alpha_2, \tag{13}$$

$R_1+R_2\neq\sqrt{3}\omega\left(L_1+L_2\right)$ – third-order invariant,

$$\sqrt{2}\omega\left(R_1+R_2\right)\neq\alpha_1+\alpha_2,\ \sqrt{2}\left(R_1+R_2\right)\neq\omega\left(L_1+L_2\right)\ \text{or}$$
$$\omega^2\left(R_1+R_2\right)^4-5\left(\alpha_1+\alpha_2\right)^2\left[2\left(R_1+R_2\right)^2\omega^2-\left(\alpha_1+\alpha_2\right)^2\right]\neq 0, \tag{14}$$

$\left(R_1+R_2\right)^4-5\omega^2\left(L_1+L_2\right)^2\left[2\left(R_1+R_2\right)^2-\omega^2\left(L_1+L_2\right)^2\right]\neq 0$ – fourth-order invariant.

In the general form, the condition for existence:

$$\left[\omega^2\left(R_1+R_2\right)^2+\left(\alpha_1+\alpha_2\right)^2\right]\frac{\partial}{\partial\omega}\left[f_n\left(\alpha_1,\alpha_2,R_1,R_2,\omega\right)\right]\neq$$
$$\neq 2\omega(n+1)\left(\alpha_1+\alpha_2\right)^2 f_n\left(\alpha_1,\alpha_2,R_1,R_2,\omega\right);$$
$$\left[\left(R_1+R_2\right)^2+\omega^2\left(L_1+L_2\right)^2\right]\frac{\partial}{\partial\omega}\left[f_n\left(L_1,L_2,R_1,R_2,\omega\right)\right]\neq \tag{15}$$
$$\neq 2\omega(n+1)\left(L_1+L_2\right)^2 f_n\left(L_1,L_2,R_1,R_2,\omega\right).$$

Let us determine conditions for the existence of invariants according to increments. Second-order increment (otherwise –finite differences of the second order [4]) can be determined as:

$$\frac{\Delta^2\tilde{N}}{\Delta^2 g}=\frac{\dfrac{\Delta\tilde{N}_{\omega 2}-\Delta\tilde{N}_{\omega 1}}{\Delta\omega_2-\Delta\omega_1}}{\dfrac{\Delta g_{\omega 2}-\Delta g_{\omega 1}}{\Delta\omega_2-\Delta\omega_1}}=\frac{\dfrac{\tilde{N}_3-\tilde{N}_2-\left(\tilde{N}_2-\tilde{N}_1\right)}{\omega_3-\omega_2-\left(\omega_2-\omega_1\right)}}{\dfrac{g_3-g_2-\left(g_2-g_1\right)}{\omega_3-\omega_2-\left(\omega_2-\omega_1\right)}}=\frac{-\dfrac{\left(\tilde{N}_1+\tilde{N}_2\right)\left(\tilde{N}_1g_2-\tilde{N}_2g_1\right)^2\left(\omega_3-\omega_1\right)\times}{\left(\omega_3+\omega_1-2\omega_2\right)\times}\rightarrow}{\dfrac{\left(g_1+g_2\right)\left(\tilde{N}_1g_2-\tilde{N}_2g_1\right)^2\left(\omega_3-\omega_1\right)\times}{\left(\omega_3+\omega_1-2\omega_2\right)\times}\rightarrow}\rightarrow$$
$$\rightarrow\frac{\times\left\{\left(g_1+g_2\right)^2-\left(\tilde{N}_1+\tilde{N}_2\right)^2\left[\omega_2\left(\omega_3+\omega_1\right)+\omega_3\omega_1\right]\right\}}{\times\prod_{i=1}^{3}\left[\left(g_1+g_2\right)^2-\omega_i^2\left(\tilde{N}_1+\tilde{N}_2\right)^2\right]}$$
$$\rightarrow\frac{\times\left\{\left(g_1+g_2\right)^2-\left(\tilde{N}_1+\tilde{N}_2\right)^2\left[\omega_2\left(\omega_3+\omega_1\right)+\omega_3\omega_1\right]\right\}}{\times\prod_{i=1}^{3}\left[\left(g_1+g_2\right)^2-\omega_i^2\left(\tilde{N}_1+\tilde{N}_2\right)^2\right]}=\frac{\tilde{N}_1+\tilde{N}_2}{g_1+g_2}, \tag{16}$$

where $C_1, C_2, C_3, g_1, g_2, g_3$ –values *C* and *g*, respectively, at frequencies $\omega_1, \omega_2, \omega_3$.

The condition for existence in this case:

$$\left(g_1+g_2\right)^2\neq\left(\tilde{N}_1+\tilde{N}_2\right)^2\left[\omega_2\left(\omega_3+\omega_1\right)+\omega_3\omega_1\right]. \tag{17}$$

Analogously, for other invariants:

$$\frac{\Delta^2\alpha}{\Delta^2 R}=-\frac{\alpha_1+\alpha_2}{R_1+R_2};\qquad\frac{\Delta^2 L}{\Delta^2 R}=-\frac{L_1+L_2}{R_1+R_2}, \tag{18}$$

conditions for existence:

$$\begin{aligned}&\left(\alpha_1+\alpha_2\right)^2\neq\left(R_1+R_2\right)^2\left[\omega_2\left(\omega_3+\omega_1\right)+\omega_3\omega_1\right];\\&\left(R_1+R_2\right)^2\neq\left(L_1+L_2\right)^2\left[\omega_2\left(\omega_3+\omega_1\right)+\omega_3\omega_1\right].\end{aligned}\tag{19}$$

Obviously, value $\omega_2\left(\omega_3+\omega_1\right)+\omega_3\omega_1$ at approximation $\Delta\omega\to 0$, where $\omega_3=\omega_2+\Delta\omega=\omega_1+2\Delta\omega$ tends to value $3\omega^2$ then conditions (17) and (19) turn into (5) and (12), which confirms the correctness of the performed transformations.

For increments of any *n*-th order, the condition for the existence of an invariant is of the form, e.g. with respect to *C* and *g*,

$$f_n\left(C_1,C_2,g_1,g_2,\omega_1\div\omega_{n+1}\right)\neq 0.\tag{20}$$

It should be noted that invariants also exist in mutual transformations of increments into differentials and differentials into increments, i.e. (omitting lengthy intermediate transformations):

$$\begin{aligned}&\frac{\Delta\left(\partial C\right)}{\Delta\left(g\right)}=\frac{\partial\left(\Delta C\right)}{\partial\left(\Delta g\right)}=-\frac{C_1+C_2}{g_1+g_2};\quad \frac{\Delta\left(\partial\alpha\right)}{\Delta\left(\partial R\right)}=\frac{\partial\left(\Delta\alpha\right)}{\partial\left(\Delta R\right)}=-\frac{\alpha_1+\alpha_2}{R_1+R_2};\\&\frac{\Delta\left(\partial L\right)}{\Delta\left(\partial R\right)}=\frac{\partial\left(\Delta L\right)}{\partial\left(\Delta R\right)}=-\frac{L_1+L_2}{R_1+R_2}.\end{aligned}\tag{21}$$

In this case, the condition for existence of an invariant e.g. with respect to *C* and *g* in transformations of increments into derivatives:

$$\left(g_1+g_2\right)^4\neq 2\omega_1\omega_2\left(\tilde{N}_1+\tilde{N}_2\right)^2\left[\left(g_1+g_2\right)^2+\left(\omega_1^2+\omega_1\omega_2+\omega_2^2\right)\left(\tilde{N}_1+\tilde{N}_2\right)^2\right],\tag{22}$$

and transformation of derivatives into increments provide an invariant existing at any positive real values C_1, C_2, g_1, g_2 (meeting (2).

Analogous results also take place for circuits б,*R,* and *L*, *R*.

3 CONCLUSIONS

Conditions for the existence of invariants of a four-element dipole with active-reactive components at differential transformations and in increments of any order and also for mutual differential-difference transformations have been determined.

References

[1] **B. I. Nevzlin:** *Identification and application of an electromagnetic invariant of a mathematical model of the controlled environment with active-reactive components,* Herald of East-Ukrainian State. Univ., Iss. 2, p.p. 155–161, 1997

[2] **B. I. Nevzlin:** *About extension of the scope of existence of an electromagnetic invariant*, Herald of East-Ukrainian State. Univ., Iss. 4., p.p. 12–14, 1997

[3] Mathematical encyclopedia. – M. : Sov. Encyclopedia, Vol. 3, p.p. 563–564, 1982

[4] Mathematical encyclopedia. – M. : Sov. Encyclopedia, Vol. 2, p.p. 1026, 1979

Journal of Energy Technology

JET Volume 8 (2015) p.p. 17-30
Issue 2, October 2015
Typology of article 1.01
www.fe.um.si/en/jet.html

THE INVERTED DISTORTED PARABOLA-LIKE SHAPE OF THE BIAS-DEPENDENT ELECTRIC FIELD AT AN ELECTRON-INJECTING METAL/ORGANIC INTERFACE DEDUCED USING THE CURRENT-VOLTAGE METHOD

OBRNJENA, DEFORMIRANI PARABOLI PODOBNA ODVISNOST ELEKTRIČNEGA POLJA OD PRITISNJENE NAPETOSTI NA VMESNI PLOSKVI KOVINA/ORGANSKI POLPREVODNIK IZPELJANA Z UPORABO METODE TOKOVNE KARAKTERISTIKE

Matjaž Koželj[R], Bruno Cvikl[1]

Keywords: Metal-organic interface, Electric field, Bias-dependent interfacial field, Current density modelling, Effective electron mobility, Organic semiconductors

Abstract

Using the recently derived expression for the traditional Mott-Gurney charge-drift model extended by the non-zero electric field at the charge-injecting interface E_{int}, the published dependence of the

[R] Corresponding author: Matjaž Koželj, MSc, Tel.: +386 1 588 5277, Fax: +386 1 588 5376, Mailing address: Jožef Stefan Institute, Jamova 39, SI-1000 Ljubljana, Slovenia
E-mail address: matjaz.kozelj@ijs.si

[1] Jožef Stefan Institute, Jamova 39, 1000 Ljubljana, Slovenia, and University of Maribor, Faculty of Energy Technology, Hočevarjev trg 1, 8270 Krško, Slovenia

current density on the applied electric field $j–E_a$ for two good-ohmic-contact, electron-only, metal/organic structures is analysed. It is argued that the Mott-Gurney law with the well-known empirical exponential bias-dependent mobility included, in spite of a very good fit to the $j–E_a$ measurements, represents an unsatisfactory method for data analyses. It is shown that the internal electric field at the electron-injecting interface is strongly bias dependent, and in such a way is coupled to the electron current within the organic bulk. The bias dependence of the interfacial field resembles an inverted, distorted, parabola-like-shaped curve, the maximum of which is organic-material dependent. Beyond the maximum, which occurs at high values of the externally applied electric field E_a, the interfacial electric field E_{int} exhibits a rapid decrease towards zero, and only at this limit can the traditional Mott-Gurney law be applied. In contrast to the present notion, it is found that the (large) electron effective mobility for the two samples investigated does not change with the bias, but it is the total effective mobility (its product with the specific non-linear algebraic function of E_a) that is bias dependent. The effective mobility may be uniquely determined, providing the applied electric field spans a sufficiently wide E_a interval. It is argued that an appropriate width of this interval may be tested by the judicious application of the derived expression in the limit $E_{int} \to 0$. The Alq_3 bias-dependent interfacial electric field at the electron injecting cathode/organic junction results in a non-linear response of the corresponding free electron density, $n_{free}(L=200\ nm)$, at this site. The possibility for an investigation of the electric field at the charge-injecting metal/organic interface using the $j–V$ method is therefore outlined.

Povzetek

V prispevku je analizirana odvisnost tokovne gostote od pritisnjenega električnega polja $j–E_a$ za primer dveh struktur kovina/organski polprevodnik, katerih značilnost so dobri ohmski kontakti in elektronsko prevajanje toka, pri čemer smo uporabili nedavno izpeljano enačbo za konvencionalni Mott-Gurney model dopolnjen z od nič različnim električnim poljem na vmesni ploskvi. Dokazano je, da Mott-Gurneyev zakon z vključeno empirično eksponentno odvisnostjo, kljub dobrem ujemanju z j-E_a meritvami, ne predstavlja zadovoljivo metodo za analizo podatkov. Pokazali smo, da je električno polje na vmesni ploskvi, na kateri poteka vbrizgavanje elektronov, močno odvisno od pritisnjene napetosti in tako povezano z elektronskim tokom skozi organski polprevodnik. Odvisnost električnega polja od pritisnjene napetosti je podobna obrnjeni, deformirani paraboli podobni krivulji, katere maksimum je odvisen od vrste organskega materiala. Konvencionalni Mott-Gurneyev zakon je možno uporabiti v limiti, ko električno polje na vmesni ploskvi, E_{int}, preseže maksimum in se potem hitro zmanjša do nule, kar se zgodi pri visokih vrednostih pritisnjene napetosti. Za razliko od trenutno veljavne razlage smo ugotovili, da se (velika) efektivna elektronska mobilnost v dveh raziskanih vzorcih ne spreminja s pritisnjeno napetostjo, pač pa je celotna efektivna mobilnost (produkt efektivne mobilnosti s specifično nelinearno algebraično funkcijo E_a) odvisna od pritisnjene napetosti. Efektivno mobilnost je možno določiti izključno pod pogojem, da se pritisnjeno električno polje spreminja v dovolj širokem intervalu. Dokazano je, da je primernost tega intervala možno preveriti s primerno uporabo izpeljanega izraza v limiti $E_{int} \to 0$. Električno polje na vmesni ploskvi katoda/organski polprevodnik Alq_3, na kateri poteka vbrizgavanje elektronov, ki je odvisno od pritisnjene napetosti, ima za posledico nelinearni odziv ustrezne gostote prostih elektronov, $n_{free}(L=200\ nm)$, na tem mestu. Podana je možnost za raziskave električnega polja na vmesni ploskvi kovina/organski polprevodnik, kjer poteka vbrizgavanje naboja, s pomočjo $j–V$ metode.

1 INTRODUCTION

An understanding of the intrinsic charge-transport properties is vital to the optimum operation of any electronic device that is based on organic semiconductors. Such devices currently used in practical applications include flat-panel displays, organic solar cells, flexible electronics, solid-state lighting, etc. An important step towards the widespread additional application of organic electronic devices is the continuous striving for a fuller understanding of the numerous factors that are currently limiting their performance. Considerable research has been devoted to uncovering the exact operation mechanisms of such devices and to a precise determination of their electrical and optical properties. In this respect, two important issues that have received a great deal of attention recently are the effects of the organic electron and hole layers on the efficiencies of devices, [1], and the exact role of chemical impurities, [2], which may either hinder or enhance the performance of the device. Both issues are intimately related to an investigation of the intrinsic charge-carrier mobility, [3-5], which is often measured using the current-voltage method, admittance spectroscopy, the time-of-flight method and transient electroluminescence.

This work is focused on a determination of the electron mobility within a single organic layer using the current-voltage method. It represents the extension of a related investigation on hole charge carrying, [6], with the aim being to dispense with the charge-density singularity at the charge-injecting metal/organic interface that characterizes the well-known Mott-Gurney law. The Mott-Gurney expression, incorporated with the empirical exponential bias-dependent mobility, [7], is of paramount importance for the charge-carrier mobility determination using the current-voltage method.

It has been shown recently, [6], that the existence of a non-zero interfacial electric field at the charge-injecting metal/organic junction causes the extinction of the singularity of the free-charge density that the Mott-Gurney law predicts. The investigation of the published *j–V* data obtained on two distinct organic structures, characterized by a series of single organic layers that differ in thickness, has shown that the effective hole mobility (to be distinguished from the total hole mobility) is bias independent. It was shown in the literature that the well-known empirical exponential bias-dependent mobility, [7], is an artefact that should be replaced by a derived, non-linear algebraic expression that depends only on the ratio of the interfacial field to the externally applied electric field [6].

However, assuming a non-zero bias-independent interfacial electric field at the *electron-injecting* cathode/organic interface, E_{int}, it is not possible to describe the electron-only current-voltage, *j–V*, data of the good-ohmic-contact, single-layer organic structures of Yasuda et al., [8]. However, these data have been analysed by the authors in terms of the Mott-Gurney law that includes the empirical exponential bias-dependent mobility, and a very good fit was obtained; see Figs. 4 and 5 of Ref. [8].

In this work, it is shown that the electron-only current density within the two organic structures investigated in Ref. [8] is strongly coupled to the bias-dependent internal electric field existing at the electron-injecting interface. The bias dependence of the interfacial electric field, E_{int}, is explicitly revealed for the published *j–V* data [8] for two metal/organic structures. For small applied fields E_a, it is shown that the interfacial electric field of both structures coincides and exhibits a *linear increase* with an increasing external electric field E_a, a behaviour that is apparently independent of the organic composition. At a certain value of E_a, which is organic-material dependent, the straight line transforms into an inverted distorted parabola-like curve,

rapidly decreasing to a value close to zero. This small value of E_{int} apparently occurs when the last, the maximum, value of the current density in the *j–V* diagram is reached. If E_{int} turns out to be negligibly small at the maximum value E_a^{max} of the E_a interval, then the traditional Mott-Gurney limit is attained. The effective mobility within the electron-only, single-layer, metal/organic structure investigated in this work turns out to be bias independent. As shown earlier in [6], apart from the E_a^2 term, the *additional external bias dependence* of the current density is provided by the previously derived, non-linear algebraic function of the argument $\lambda(E_a) = \frac{E_{\text{int}}(E_a)}{E_a}$, which is implicitly and explicitly dependent on the external electric field. This fact offers an indication that the processes that determine the electron mobility differ from the ones that determine the hole mobility. In this work, it is once again confirmed that the empirical exponential bias-dependent function for the effective mobility is redundant, within the range of the *j–V* measurements.

2 THEORETICAL OUTLINE

It can be easily verified that the drift-current density in a single-layer organic structure is, irrespective of the sign of the charge carriers, described by the expression, [6],

$$j = \frac{\varepsilon\varepsilon_0\mu_{eff}}{2L} E_a^2 \left[\frac{9}{8} - \frac{3}{2}\lambda^2 + \left(\frac{81}{64} - \frac{3}{4}\lambda^4 + 3\lambda^3 - \frac{27}{8}\lambda^2\right)^{\frac{1}{2}}\right] \tag{2.1}$$

where E_a is the externally applied electric field, defined as $E_a = V_a/L$, and V_a is the applied bias on the anode placed at the origin of the frame of reference (the cathode at $x = L$ is at zero potential), j is the current density through the metal/organic structure, μ_{eff} is the effective mobility, ε is the dielectric constant and ε_0 is the permittivity of free space, [6]. The current density, j, Eq. (2.1) replaces the well-known generalized Mott-Gurney model (in the sense that the empirical, [7], exponential bias-dependent charge mobility is included in the expression) of charged traps in the organic layer for completely empty (or equivalently, completely full) or the stated model, if the *non-zero interfacial electric field*, E_{int}, occurring at the charge-injecting metal/organic interface is taken into account. Here, the parameter λ denotes the ratio of the *non-zero* electric field at the charge-injecting interface, E_{int}, to the externally applied electric field, E_a,

$$\lambda = \frac{E_{\text{int}}}{E_a} \tag{2.2}$$

where E_{int} might be bias dependent The introduction of the interfacial field results in the disappearance of the free-charge-density singularity at the stated interface, a serious shortcoming of the above-mentioned, generalized Mott-Gurney model. Of equal importance is the fact that in Eq. (2.1) the effective mobility μ_{eff} is bias independent and the bias dependence is described in terms of the non-linear algebraic expression, which is a function of the parameter λ. Evidently, for $E_{int} = 0$, Eq. (2.1) reduces to the (original) Mott-Gurney model with a bias-independent effective mobility. In Ref. [6], Eq. (2.1) was tested on the published *j–V* data obtained on two different sets of single-layer, hole-only, metal/organic structures and good agreements with the measurements were obtained. For holes, it was shown that the interfacial electric field is bias independent and just slightly smaller than the initial value of the externally applied electric field. It was also explicitly shown that the effective mobility of the holes is thickness dependent,

but bias independent. Furthermore, it was shown that the empirical exponential bias-dependent effective hole mobility is redundant in *j–V* experiments since it represents merely an approximation of the derived algebraic expression represented by Eq. (2.1).

It can be easily shown that the expression for the current density *j*, i.e., Eq. (2.1), is invariant with respect to the sign of a drifting charge carrier within a single organic layer and is consequently also valid for electrons. Consequently, the spatial dependence of the internal electric field *E(x)* reads,

$$E(x) = \sqrt{E_{\text{int}}^{\,2} + \frac{2j(E_a)}{\varepsilon\varepsilon_0\mu_{eff}}(L-x)} \tag{2.3}$$

and the spatial dependence of the electric potential *V(x)*, taking into account that *V(L)* = 0, is then:

$$V(x) = \frac{\varepsilon\varepsilon_0\mu_{eff}}{3j(E_a)}\left\{\left[E_{\text{int}}^2 + \frac{2\varepsilon\varepsilon_0\mu_{eff}}{j(E_a)}(L-x)\right]^{\frac{3}{2}} - E_{\text{int}}^3\right\} \tag{2.4}$$

and the free-electron (number) density $n_f(x)$ reads:

$$n_f(x) = -\frac{\varepsilon\varepsilon_0\theta}{q}\frac{dE(x)}{dx} = \frac{j(E_a)\theta}{q\mu_{eff}}\frac{1}{\left[E_{\text{int}}^2 + \frac{2j(E_a)}{\varepsilon\varepsilon_0\mu_{eff}}(L-x)\right]^{1/2}} \tag{2.5}$$

In Eq. (2.5) ϑ denotes the ratio of the free to the total (free and the bound) charge densities [9], $\vartheta = \frac{n_f}{(n_f + n_b)}$ and the effective mobility [9] is defined as $\mu_{eff} = \mu\,\vartheta$.

Evidently, in the limit $E_{int} = 0$, Eq. (2.1) reduces to:

$$j(E_a) = \frac{9}{8}\frac{\varepsilon\varepsilon_0\mu_{eff}}{L}E_a^2 \tag{2.6}$$

the well-known Mott-Gurney expression, which in combination with the empirical exponential bias-dependent mobility of Gil, [7]

$$\mu_{eff} = \mu_0 \exp\left(\gamma\sqrt{E_a}\right) \tag{2.7}$$

has been in current-voltage, *j–V*, experiments exclusively used for the determination of the charge mobility. For $E_{int} \neq 0$, the curve evaluated by the combination of Eqs. (2.6) and (2.7) may, within the relevant interval of E_a, coincide with Eq. (2.1), see Ref. [6]. Here, the two parameters μ_0 and γ are determined from the fit to the experimental data, but have no clear physical meaning. However, as pointed out in Ref. [6], the combination of Eqs. (2.6) and (2.7) is incomplete, exhibiting a singularity of the free-charge density at the charge-injecting interface, see Eq. (2.5), and it should be substituted by the corresponding Eq. (2.1). This assertion was already empirically proved for hole charge carriers, [6], and so its extension to the electron current density is the subject of the work presented here.

3 BIAS DEPENDENCE OF THE INTERFACIAL ELECTRIC FIELD

Yasuda et al. [8] used the current-voltage method to investigate the electron mobility of six different electron-only, single-layer organic structures characterized by a quasi-ohmic contact. It should be emphasized that all the data were analysed in terms of Eqs. (2.6) and (2.7), since an excellent agreement between the calculated curves and the measurements was obtained, see Figs. 4 and 5 of Ref. [8]. For the purposes of this work, the interval of the externally applied electric field constitutes indispensable information for the application of Eq. (2.1). For two of the six organic structures, i.e., tris-(8-hydroxyquinoline), denoted as Alq_3, and 2,9-dimethyl-4,7-diphenyl-1,10-phenanthroline, known as the BCP organic material, this information is clearly revealed, see Figure 2 of Ref. [8]. As a result of the excellent agreement between the data and the calculated fit shown in Ref. [8], in this work the data will be represented in terms of Eqs. (2.6), and (2.7) for the following values of the parameters, [8]: $\mu_0 = 4.7 \times 10^{-13}$ m^2/Vs and $\gamma = 6.9 \times 10^{-4}$ (m/V)$^{1/2}$ valid within the interval of the bias 1 V $\leq V_a \leq$ 20 V for the Alq_3 organic, and $\mu_0 = 2.3 \times 10^{-12}$ m^2/Vs and $\gamma = 11.0 \times 10^{-4}$ (m/V)$^{1/2}$ valid within the interval of the bias 3 V $\leq V_a \leq$ 15 V for the BCP structure. In both cases, an average value [8] L = 200 nm was taken as the layer thickness in the calculations.

It is clear that because of the considerable disagreement between the two curves shown in Figure 1, the interfacial electric field E_{int} may not be constant in the experiment of Yasuda et al. [8]. In order to test the hypothesis, the current density of Eq. (2.1) at a given E_a should equal the corresponding data (i.e., using Eqs. (2.6), and (2.7) for convenience) and the parameter λ is then deduced as a real root of the expression,

$$\mu_{eff}\left[\frac{9}{8}-\frac{3}{2}\lambda^2+\left(\frac{81}{64}-\frac{3}{4}\lambda^4+3\lambda^3-\frac{27}{8}\lambda^2\right)^{\frac{1}{2}}\right] = \frac{9}{4}\,\mu_0 \exp\left(\gamma\sqrt{E_a}\right) \tag{3.1}$$

The obtained value of λ and the associated value of the interfacial electric field at the electron-injecting interface E_{int} are presented in Table 1. Using these values in Eq. (2.1), the two curves presented in Figure 1 then coincide to an excellent degree. The deduced bias dependence of E_{int} for the Alq_3 organic (circles) is presented in Figure 2.

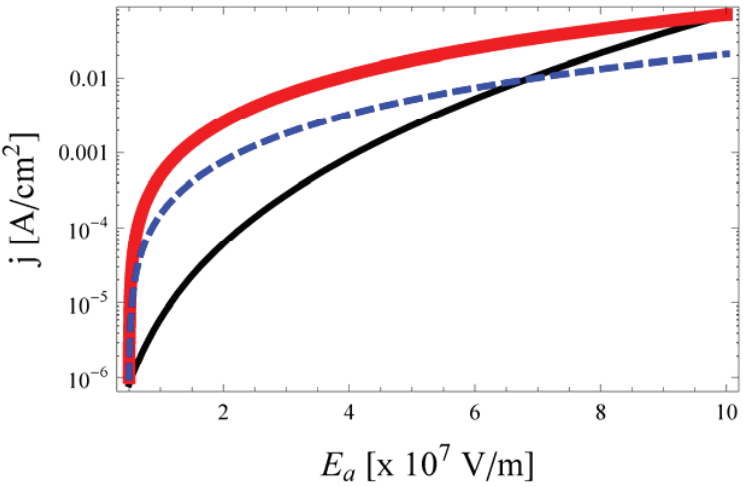

Figure 1: *The room-temperature j–E_a data of the electron-only, good-ohmic-contact, Al/Alq_3(200 nm) structure are within the complete interval 5 MV/m ≤ E_a ≤ 100 MV/m presented in the analytical form (thin line) of Ref. [8]. For fixed, i.e., bias-independent, parameters μ_{eff} = 4.7 × 10^{-10} m²/Vs and E_{int} = 4.986 MV/m, the current density calculated from Eq. (2.1) matches the data only at the initial and at the end value of the E_a interval (thick line). Assuming the interfacial electric field at the electron-ejecting contact E_{int} to be E_a dependent, then a practically exact match with the corresponding experimental current-density data is obtained. The dashed curve presents the results of Eq. (2.1) within the shortened E_a interval, i.e., 5 MV/m ≤ E_a ≤ 60 MV/m. The curve calculated for the fixed parameters μ_{eff} = 1.4 × 10^{-10} m²/Vs and E_{int} = 4.956 MV/m, which also intersects the data at the initial value of the current density, illustrates the dependence of the deduced effective mobility on the width of the E_a interval considered.*

Table 1: *From Eq. (3.1), the calculated dependence of the internal electric field, E_{int}, on the externally applied electric field, E_a, at the electron-ejecting good-ohmic-contact Al-Liac/Alq_3(200 nm) interface based on the room-temperature j-V data of Ref. [8] is presented. For comparison, taking the initial, bias independent value of the interfacial electric field $E_{int}^{ini} = 4.986$ MV/m, with a bias-independent effective mobility within the Alq_3 organic layer equal to $\mu_{eff} = 4.7 \times 10^{-10}$ m²/Vs, then the resulting curve, Eq. (2.1) (thick line), intersects the measurements, [8], only at two points, the data endpoints, Figure 1. Consequently, the deduced E_a dependence of E_{int} is presented in Figure 2 as the distorted inverted-parabola-like curve and the resulting current density (last column) as a function of E_a then practically exactly reproduces the analytical data description of Ref. [8] in terms of Eqs. (2.6) and (2.7).*

E_a [× 10^7 V/m]	λ	E_{int} [× 10^7 V/m]	j [A/cm²]
	Alq_3 L = 200 nm thick layer	**μ_{eff} = 4.7 × 10^{-10} m²/Vs**	
0.5	0.9974	0.4986	8.224×10^{-7}
1.0	0.9950	0.9950	6.225×10^{-6}
2.0	0.9876	1.9753	6.135×10^{-5}
3.0	0.9752	2.9255	2.764×10^{-4}
4.0	0.9551	3.8205	8.819×10^{-4}
5.0	0.9241	4.6203	2.306×10^{-3}
6.0	0.8769	5.2614	5.291×10^{-3}
7.0	0.8058	5.6408	1.105×10^{-2}
8.0	0.6972	5.5773	2.150×10^{-2}
9.0	0.5204	4.6839	3.957×10^{-2}
10.0	0.07736	0.7737	6.961×10^{-2}

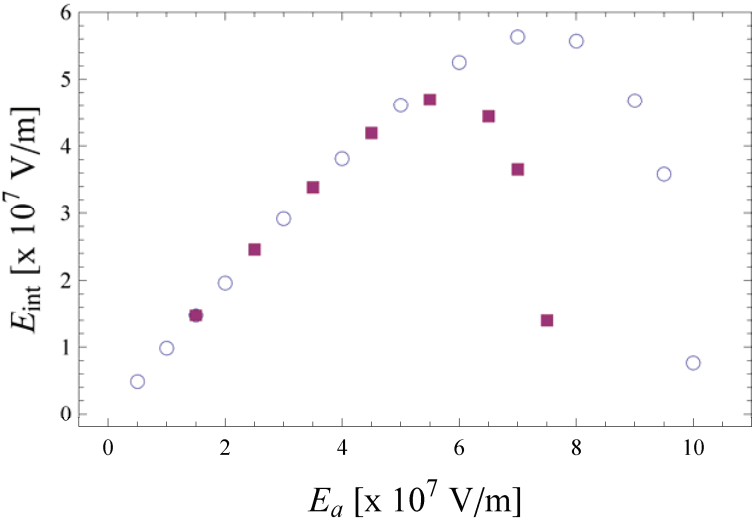

Figure 2: *The evaluated interfacial electric field E_{int}, see Eq. (3.1), at the electron-injecting metal/organic interface as a function of the externally applied electric field E_a is presented. The circles refer to the 200 nm-thick Alq_3 layer, and the filled boxes refer to the 200 nm-thick BCP layer. The calculated results are characterized by the inverted distorted-parabola-like curve, which, within the range of small values of the externally applied electric field, coincides and exhibits an identical linear E_a dependence.*

Figure 3 shows the calculated spatial dependence of the internal electric field, *E(x)*, for a 200 nm-thick Alq_3 organic layer for externally applied electric fields of E_a = 60 MV/m (dashed line) and 100 MV/m (dash-dot curve). The calculated spatial dependence of the corresponding free electron (number) density, $n_{free}(x)$, is shown in Figure 4. The calculated bias dependence of the free-electron density, $n_{free}(L=200\ nm)$, at the electron-injecting cathode/organic junction for the Alq_3 organic structure, taking into account the bias-dependent interfacial electric field of Figure 2, is presented in Figure 5.

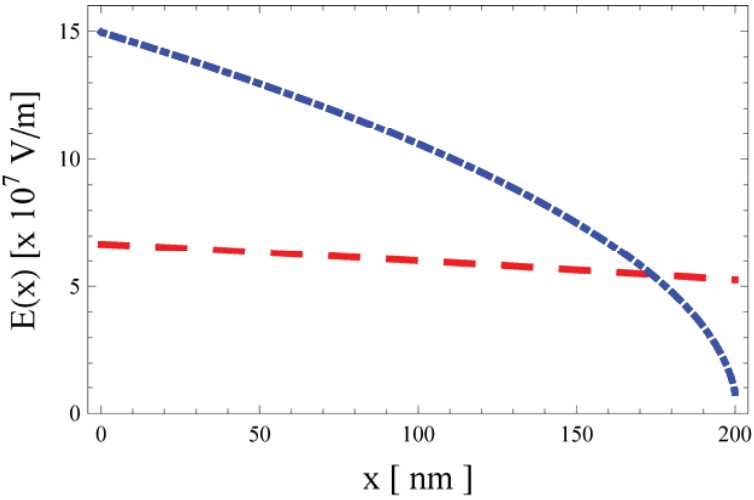

Figure 3: *The calculated spatial dependence of the internal electric field, E(x) for L = 200 nm-thick Alq_3 organic layer for two values of the externally applied electric field E_a is shown. (a) E_a = 60 MV/m (dashed line), and (b) E_a = 100 MV/m (dash-dot line). The corresponding value of the non-zero interface electric field is given in Table 1. The anode is placed at the origin, and the cathode is located at x = 200 nm.*

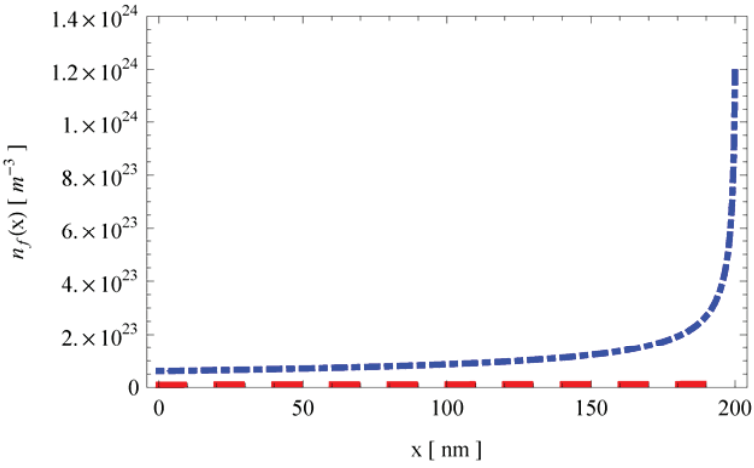

Figure 4: *The detail of the calculated spatial dependence of the free-electron (number) density $n_{free}(x)$ for the L = 200 nm-thick Alq_3 organic layer for the two values of the externally applied electric field E_a is shown. (a) E_a = 60 MV/m (dashed line), and (b) E_a = 100 MV/m (dash-dot line). The finite values of the corresponding electron charge density at both interfaces are: (a) $n_{free}(x=0) = 1.05 \times 10^{22}$ m^{-3}, and $n_{free}(x=200\ nm) = 1.34 \times 10^{22}$ m^{-3}, and (b) $n_{free}(0) = 6.19 \times 10^{22}$ m^{-3}, and $n_{free}(x=200\ nm) = 1.20 \times 10^{24}$ m^{-3}. No evidence of the space charge limited current for E_a < 60 MV/m is exhibited. The anode is placed at the origin, and the cathode is located at x = 200 nm.*

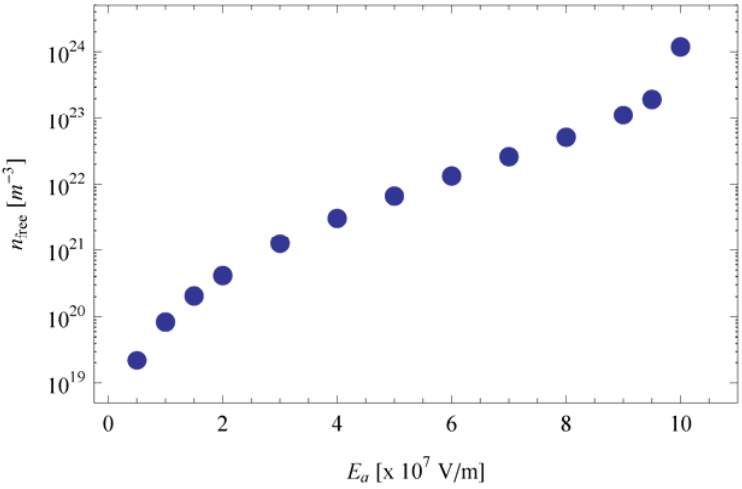

Figure 5: *The calculated bias dependence of the free-electron density, n_{free}(L=200 nm), at the electron-injecting cathode/organic junction for the Alq_3 organic structure, taking into account the bias-dependent interfacial electric field of Figure 2 is shown.*

A similar analysis can be made for the BCP structure within the interval of 15 MV/m $\leq E_a \leq$ 75 MV/m. Analogous to the above-described steps, the parameters of the curve evaluated by Eq. (2.1) through both endpoints of the complete E_a interval were found to be: $\mu_{eff} = 3.3 \times 10^{-8}$ m^2/Vs, and (the initial) E_{int} = 14.958 MV/m. In Table 2, the roots of λ and the associated E_{int} deduced from Eq. (3.1) together with the corresponding current density, Eq. (2.1), are presented, and the bias variation of the BCP interfacial electric field is depicted in Figure 2. As is clear from Figure 2, the interfacial electric field E_{int} for both organic structures exhibits, within the linear increase, practically identical behaviour, i.e., both calculated curves coincide and are linearly increasing functions of E_a. For a given value of E_a, which is organic-material dependent, the linear function transcends into an inverted-parabola-like behaviour, characterized by a rapid decrease in the interfacial field E_{int} towards zero. The maximum of the inverted-parabola-like curve occurs at E_a, which as is clear from Figure 2, is organic-material dependent. By using such deduced values of λ for each of the described two cases in Eq. (2.1), the experimental data are fully recovered. The bias-independent value of the deduced effective mobility, μ_{eff}, is clearly noted as well as the incompatibility with the corresponding result obtained on the basis of Eqs. (2.6) and (2.7).

Table 2: *From Eq. (3.1), the calculated dependence of the internal electric field, E_{int}, on the externally applied electric field, E_a, at the electron-ejecting good-ohmic-contact Al-Liac/BCP(200 nm) interface based on the room-temperature j–V data of Ref. [8] is presented. The calculated E_a dependence of E_{int} is presented in Fig. 2 as the distorted inverted-parabola-like curve and the resulting current density (last column) as a function of E_a then to an excellent approximation reproduces the analytical data description [8] in terms of Eqs. (2.6) and (2.7).*

E_a [× 10^7 V/m]	λ	E_{int} [× 10^7 V/m]	j [A/cm²]
	BCP L = 200 nm thick layer	**μ_{eff} = 3.3 × 10^{-8} m²/Vs**	
1.5	0.9972	1.4958	5.512×10^{-4}
2.5	0.9904	2.4759	5.259×10^{-3}
3.5	0.9735	3.4072	2.819×10^{-2}
4.5	0.9358	4.2111	0.112
5.5	0.8559	4.7075	0.362
6.5	0.6852	4.4539	1.030
7.5	0.1887	1.4149	2.648

On the basis of the above-presented results, we are led to the conclusion that the electron-only current density for both good-ohmic-contact structures of Ref. [8], i.e., the Al-Liac/Alq_3(200 nm) and the Al-Liac/BCP (200 nm), is strongly coupled by the non-zero bias-dependent electric field existing at the cathode/organic interface. Here, Al-Liac denotes the 40 nm-thick layer of Al with a 2 nm-thick buffer layer of lithium acetylacetonate serving as the cathode in contact with the organic layer of interest, [8].

Regarding the magnitude of the bias-independent effective electron mobility in Alq_3 and BCP, we observe that it is roughly of the same order of magnitude as the (thickness-dependent but bias-independent) hole mobility. At this point, the apparent contradiction between the stated claim and the literature reports, according to which the bias-dependent electron mobility is measured in general, deserves a comment. From examining Eq. (2.1), we see that the *total mobility* is a product of the bias-independent effective mobility, as referred to in this work, and a non-linear algebraic function of the applied field E_a.

$$M_{tot} = \mu_{eff}\left[\frac{9}{8}-\frac{3}{2}\lambda^2+\left(\frac{81}{64}-\frac{3}{4}\lambda^4+3\lambda^3-\frac{27}{8}\lambda^2\right)^{\frac{1}{2}}\right] \tag{3.2}$$

Evidently, the total mobility M_{tot} is, therefore, E_a dependent and apparently it is this bias dependence that is measured in *j–V* and similar experiments, although this fact is not recognized in the literature.

4 UNIQUENESS OF THE DEDUCED μ_{EFF}

The above-presented method for the experimental determination of the effective mobility strongly depends on the width of the E_a interval, resulting in a given set of current-voltage data. This means that one has to know, to a good approximation, the maximum value of E_a at which Eqs. (3.1) and (2.7) are no longer able to fit the data or, alternatively, the current density can no longer be measured.

Let us assume that an incomplete E_a is taken for the data analysis, as shown in Figure 1 by the dashed curve for the Alq_3 organic. The initial data point coincides with the previous one, but the end point is placed at E_a^{max} = 60 MV/m, for which the experimental current density reads j_{max} = 5.291 × 10^{-3} A/cm^2 (Table 1), while the rest of the interval is ignored. The parameters of Eq. (2.1) for which the dashed curve is passing through the stated two points are: μ_{eff} = 1.4 × 10^{-10} m^2/Vs and E_{int} = 4.956 MV/m. The new value of the effective mobility differs from the previously determined one μ_{eff} = 4.7 × 10^{-10} m^2/Vs, but E_{int} remains nearly unchanged. As seen in Figure 2 (see also Table 1), the former two values are deduced close to the upper boundary of the E_a interval, characterized by the rapid decrease towards zero of the interfacial field E_{int}. In the limit $E_{int} \rightarrow 0$, Eq. (2.1) reduces to Eq. (2.6), and we can assume that this occurs at the maximum value of the applied field $E_a = E_a^{max}$. Consequently one has:

$$\mu_{eff} = \frac{8}{9} \frac{j_{\max} L}{\varepsilon\varepsilon_0} \frac{1}{\left(E_a^{\max}\right)^2} \tag{4.1}$$

Inserting the above two values, i.e., μ_{eff} = 1.4 × 10^{-10} m²/Vs and E_a^{max} = 60 MV/m, into Eq. (4.1) means the result obtained is equal to μ_{eff} = 9.85 × 10^{-11} m²/Vs, which is in clear contradiction to the input value of μ_{eff} = 1.4 × 10^{-10} m²/Vs. The "self-consistency" test, Eq. (4.1), applied to the curve passing through the "true" end points of the E_a interval (dashed line in Figure 1) then results in μ_{eff} = 4.66 × 10^{-10} m²/Vs, which is in good agreement with the input of μ_{eff} = 4.7 × 10^{-10} m²/Vs, in spite of the fact that at 100 MV/m the corresponding E_{int} is small, but still non-zero, see Figure 2 and Table 1.

Since the E_a intervals of the four additional organic structures investigated in Ref. [8] are unfortunately not explicitly stated, this omission precludes any similar analyses.

The presented arguments then emphasize the importance that for a determination of the total effective mobility of the electron-only, good-ohmic-contact, single-layer organic structure, a set of data measured over a wide interval of bias is obtained, providing that it has a good fit with Eqs. (2.6) and (2.7) to the data. These two expressions serve as a simple approximation function for the measurement, ensuring that Eq. (2.1) may be applied with credibility. Only under such conditions is Eq. (2.1) expected to provide reliable, physically meaningful information, i.e., the magnitude of the (bias-independent) effective mobility μ_{eff} and the magnitude and bias dependence of the internal electric field at the electron-injecting cathode/organic interface, E_{int}.

5 CONCLUSIONS

Using the recently upgraded Mott-Gurney charge-drift model, as extended by the non-zero electric field at the charge-injecting interface, the experimental dependence of the current density versus the applied electric field for two good-ohmic-contact, electron-only, 200 nm-thick, Alq_3, and BCP organic layers, as published in the literature, is analysed.

It is shown that the (traditional) well-known Mott-Gurney law in combination with the empirical exponential bias-dependent electron mobility, which in fact describes the experimental j–E_a line shape to a very good approximation, represents an unsuitable method for data analysis. In the presented work, it is shown that the internal electric field at the electron-injecting interface is

strongly bias dependent, and in such a way it is coupled to the unipolar electron current within the organic layer. The bias dependence of the interfacial field resembles an inverted, distorted-parabola-like curve, the maximum of which is organic-material dependent. Beyond the maximum that occurs at high values of the externally applied electric field, the interfacial electric field rapidly decreases towards zero and only in this limit can the traditional Mott-Gurney model be applied.

It is shown that the effective electron mobility for the two samples investigated is bias independent, but its exact value may be uniquely determined, providing that the experimental electric field spans a wide enough E_a interval. As shown, the appropriate width of this interval may be tested by the judicious application of the derived expression for the drift current density.

The calculated bias dependence of the free electron density, $n_{free}(L=200\ nm)$, at the electron injecting cathode/organic junction for an Alq_3 organic structure, taking into account the bias dependent interfacial electric field, is a non-linear function of the applied electric field.

The possibility for the investigation of the electric field at the charge-injected metal/organic interface using the *j–V* method is thus outlined.

References

[1] **Hao-Wu Lin, Chih-We Lu, Li-Yen Lin, Yi-Hong Chen, Wei-Chieh Lin, Ken-Tsung Wong and Francis Lin:** *Pyridine-based electron transporting materials for highly efficient organic solar cells*, J. Mater. Chem A, Vol .1, Iss. 5, p.p. 1770-1777, 2013

[2] **Loren Kaake, Xuan-Dung Dang, Wei Lin Leond, Yuan Zhang, Alan Heeger and Thuc-Quyen Nguyen:** *Effects of Impurities on Operational Mechanism of Organic Bulk Heterejunction Solar Cells*, Adv. Mater, Vol. 25, Iss. 12, p.p. 1706-1712, 2013

[3] **Yanping Wang, Jiangshan Chen, Lisong Dong and Dongge Ma**: *Determination of electron mobility in tris(8-hydroxy-quinolinato) aluminium by admittance spectroscopy*, J. Appl. Phys., Vol. 114, Iss. 11, p.p. 113703, 2013

[4] **Sang Ho Rhee, Ki Bong Nam, Chang Su Kim, Myungkwan Song, Woosum Cho, Sung-Ho Jin and Seung Yoon Ryua:** *Effect of Electron Mobility of the Electron Transport Layer on Fluorescent Organic Light-Emitting Diodes*, ECS Solid State Letters, Vol. 3, Iss. 5, p.p. R19-R22, 2014

[5] **Qifan Yan, Yan Zhou, Yu-Qing Zheng, Jian Pei and Dahui Zhao:** *Towards rational design of organic electron acceptors for photovoltaics: astudy based on perylenediimide derivatives*, Chem. Sci., Vol. 4, Iss. 12, p.p. 4389-4394, 2013

[6] **B. Cvikl:** *The electric field at hole injecting metal/organic interfaces as a cause for manifestation of exponential bias-dependent mobility*, Thin Solid Films, Vol. 573, p.p. 56-66, 2014

[7] **W. D. Gill**: *Drift mobilities in amorphous charge-transfer complexes of trinitrofluorenone and poly-n-vinylcarbazole*, J. Appl. Phys., Vol. 43, Iss. 12, p.p. 5033-5040, 1972

[8] **Takeshi Yasuda, Yoshihisa Yamaguchi, De-Chun Zou and Tetsuo Tsutsui**: *Carrier Mobilities in Organic Electron Transport Materials Determined from Space Charge Limited Current*, Jpn. J. Appl. Phys., Vol. 41, Iss. 9R, p.p. 5626-5629, 2002

[9] **P. N. Murgatroyd:** *Theory of space-charge-limited current enhanced by Frenkel effect*, J. Phys. D: Appl. Phys., Vol. 3, Iss. 2, p.p. 151-156, 1970

Journal of Energy Technology

JET Volume 8 (2015) p.p. 31-42
Issue 2, October 2015
Typology of article 1.01
www.fe.um.si/en/jet.html

NUMERICAL AND EXPERIMENTAL INVESTIGATIONS OF TRANSIENT CAVITATING PIPE FLOW

NUMERIČNE IN EKSPERIMENTALNE RAZISKAVE PREHODNEGA KAVITACIJSKEGA TOKA V CEVI

Anton Bergant[R], Uroš Karadžić[1]

Keywords: pipe flow, transient cavitation, discrete gas cavity model, unsteady skin friction

Abstract

This paper investigates the effects of transient vaporous cavitation caused by the closure of the downstream end ball valve against the discharge. Numerical results are compared with the results of measurements in the simple reservoir-pipeline-valve apparatus. Pressures measured at the end points and at two equidistant positions along the pipeline are compared with computational results as piezometric heads. Comparisons between the results of two distinct water column separation tests and numerical simulations using an advanced discrete gas cavity model show good agreement. Two distinct column separation runs include active and passive column separation cases.

Povzetek

Prispevek obravnava prehodni parni kavitacijski tok induciran z zapiranjem dolvodnega kroglastega zapirala v sistemu pod pretokom. Računski rezultati so primerjani z rezultati meritev v preprosti preizkusni postaji, ki jo sestavljajo rezervoar, cevovod in zapiralo. Tlaki merjeni na dolvodnem in gorvodnem delu cevi in tlaka merjena na ekvidistantnih dolžinah vzdolž cevi so primerjani z izraču-

[R] Corresponding author: Anton Bergant, PhD, Litostroj Power d.o.o., Litostrojska 50, SI-1000 Ljubljana, Slovenia, anton.bergant@litostrojpower.eu

[1]Uroš Karadžić, PhD, Univerzitet Crne Gore, Mašinski fakultet, Džordža Vašingtona bb, ME-81000 Podgorica, Montenegro, uros.karadzic@ac.me

nom kot piezometrične višine. Rezultati meritev in izračunov dobljenih s pomočjo naprednega diskretnega plinskega kavitacijskega modela za dva posebna primera pretrganja kapljevinskega stebra se dobro ujemajo. Prvi primer zajema aktivno obliko pretrganja stebra, drugi primer pa predstavlja pasivno obliko pretrganja.

1 INTRODUCTION

Industrial pipeline systems operate over a broad range of operating regimes. Induced unsteady flows in pipes and system components (valve, pump, turbine) are the source of many unwanted loads in industrial installations, including severe pressure pulsations and pipeline vibrations [1], [2]. Water hammer is the propagation of pressure waves along liquid-filled pipelines, and it is caused by a change in flow velocity. The classic water hammer effect may be affected by transient cavitation, unsteady friction, fluid-structure interaction (FSI) and viscoelastic behaviour of the pipe wall [3]. Transient cavitating pipe flow occurs as a result of very low pressures during water hammer events. This paper deals with transient vaporous cavitation (column separation) that occurs when the pressure drops to the liquid vapour pressure. The amount of free and/or released gas in the liquid is assumed to be small. This is usually the case in most industrial pipeline systems. Two distinct types of transient vaporous cavitation may occur. The first type is a localized (discrete) vapour cavity with a large void fraction. A discrete vapour cavity may form at a boundary (valve, pump, turbine) or at a high point along the pipeline. In addition, an intermediate cavity may form as a result of the interaction of two low-pressure waves along the pipe. The second type of cavitation is distributed vaporous cavitation that may extend over long sections of the pipe. The void fraction for this case is small (close to zero). Distributed vaporous cavitation occurs when a rarefaction wave progressively drops the pressure in an extended region of the pipe to the liquid vapor pressure. The collapse of a vapour cavity may induce short-duration pressure pulses with values higher than the pressure initially given by the Joukowsky equation. Bergant and Simpson [4] classified column separation flow regimes regarding the physical state of the liquid and the maximum pipeline pressure as:

(i) **Active column separation flow regime.** The maximum pipeline pressure is generated following the column separation at the valve and along the pipeline (active column separation from the designer's perspective). The maximum pressure at the valve is governed by the intensity of the short duration pressure pulse.

(ii) **Passive column separation flow regime**. The maximum pipeline pressure is the water hammer pressure before intense cavitation occurs.

The value of the friction factor during unsteady flow is different than its value during steady flow. The friction factor can be expressed as a sum of two parts: 1) steady and 2) unsteady [5]. The unsteady part mimics transient-induced changes in flow conditions (velocity profile, turbulence intensity), and it is important for some unsteady flow situations. For pipelines that are not completely fixed, FSI effects have to be taken into account [6]. Viscoelastic pipe-wall behaviour is important in cases in which the pipe is made from plastic material such as high-density polyethylene [7]. Rapid filling and emptying of the pipeline may be considered to be a specific case in which both vaporous and gaseous cavities may be present [8]. Engineers should be able to predict all these events in piping systems and take appropriate measures to keep water hammer loads within the prescribed limits. There is a strong need for well-controlled

measurements of the water hammer effects; therefore, a flexible pipeline apparatus for investigating water hammer, transient cavitating flow, unsteady skin friction, fluid-structure interaction, and pipeline filling and emptying has been developed and installed at the University of Montenegro [9]. The small-scale apparatus consists of an upstream end high-pressurized tank, horizontal steel pipeline (total length 55.37 m, inner diameter 18 mm), four valve units positioned along the pipeline including the end points, and a downstream end tank (outflow tank). This paper investigates the effects of vaporous cavitation caused by the closure of the downstream end ball valve against the discharge. Comparisons between the results of two distinct water column separation tests and numerical simulations using an advanced discrete gas cavity model [10] are presented and discussed.

2 THEORETICAL MODELLING

Water hammer in liquid-filled pipelines is fully described by the continuity equation and equation of motion [1], [2],

$$\frac{\partial H}{\partial t}+\frac{a^2}{gA}\frac{\partial Q}{\partial x}=0\,, \tag{2.1}$$

$$\frac{\partial H}{\partial x}+\frac{1}{gA}\frac{\partial Q}{\partial t}+\frac{fQ|Q|}{2gDA^2}=0\,. \tag{2.2}$$

Note that all symbols are defined in the Nomenclature. Water hammer equations are valid only when the pressure is above the liquid vapour pressure. A quasi-steady approach for estimating skin friction losses (QSF) in the pipeline is satisfactory for slow transients only, [11]. Equations (2.1) and (2.2) are solved by the method of characteristics (MOC) using the staggered numerical grid, [1]. At a boundary (reservoir, valve, turbine), a device-specific equation is used instead of one of the MOC water hammer compatibility equations.

Some numerical models have been developed for simulation of transient vaporous cavitating pipe flow. One of them is a discrete gas cavity model (DGCM) that performs accurately over a broad range of input parameters [4]. The DGCM allows gas cavities to form at all computational sections within the MOC numerical grid. A liquid phase with a constant wave speed is assumed to occupy the computational reach. The DGCM is fully described by the two water hammer compatibility equations as a result of the MOC-transformation of Eqs. 2.1 and 2.2, and two additional equations; the continuity equation for the gas volume and the ideal gas equation with assumption of isothermal behaviour of the free gas, respectively, [1], [4],

$$\frac{d\forall_g}{dt}=Q_{out}-Q_{in}\,, \tag{2.3}$$

$$\forall_g=\alpha_0\forall\left(\frac{p_0^*}{p_g^*}\right). \tag{2.4}$$

The numerical solution of DGCM equations can be found elsewhere, [1], [4].

Column separation is a relatively short duration event with a wide range of rapid flow event types. For rapid transients, the unsteady friction model is needed for the proper estimation of skin friction losses during transient events, [11]. The friction factor can be expressed as a sum of the quasi-steady part f_q and the unsteady part f_u, [5]

$$f = f_q + f_u \,. \tag{2.5}$$

The quasi-steady friction factor f_q depends on the Reynolds number and relative pipe roughness. A number of unsteady friction models have been proposed in the literature including one-dimensional (1D) and two-dimensional (2D) models. In this paper, an improved convolution based unsteady friction model [12] is used in DGCM, [10]. The convolution-based model (CBM) has been analytically developed by Zielke for transient laminar flow, [13]. This model produces correct results for some flow types using analytical expressions. The unsteady friction term f_u is defined as, [12]:

$$f_u = \frac{32\nu A}{DQ|Q|}\sum_{k=1}^{N} y_k(t) \,. \tag{2.6}$$

The quantity y_k accounts for weights of past velocity changes. It is expressed as a recursive expression; theoretical derivation for y_k is given in, [12].

3 DESCRIPTION OF PIPELINE APPARATUS

A small-scale pipeline apparatus has been designed and constructed at the Faculty of Mechanical Engineering, the University of Montenegro, [9], for investigating water hammer, column separation, fluid-structure interaction, and pipeline filling and emptying. The apparatus is comprised of a horizontal pipeline that connects the upstream end high-pressurized tank and the outflow tank (steel pipe of total length L = 55.37 m; internal diameter D = 18 mm; pipe wall thickness e = 2 mm; maximum allowable pressure in the pipeline $p_{max,\,all}$ = 25 MPa) – see Fig. 1. Four valve units are positioned along the pipeline including the end points. Valve units at the upstream end tank (position 0/3) and at the two equidistant positions along the pipeline (positions 1/3 and 2/3) are comprised of two hand-operated ball valves (valves Vi/3U and Vi/3D; i = 0, 1, 2) that are connected to the intermediate pressure transducer block. Recently an additional T-section with two shut-off valves has been added to the upstream end valve unit (position 0/3) to facilitate pipeline filling and emptying tests, [14]. There are four 90° bends along the pipeline with radius R = 3D. The pipeline is anchored against the axial movement at 37 points (as close as possible to the valve units and bends). Loosening of the anchors is planned for fluid-structure interaction tests. The air pressure in the upstream end tank (total volume $\forall_{HPT}$ = 2 m³; maximum allowable pressure in the tank $p_{HPTmax,\,all}$ = 2.2 MPa) can be adjusted up to 800 kPa. The pressure in the tank is kept constant during each experimental run by using a high-precision air pressure regulator in the compressed air supply line, [9]. The upstream end tank is supplied with water from the tap water supply system. The operating air for the electro-pneumatically actuated ball valve (valve V3/3P) can be adjusted to between 200 to 400 kPa, yielding valve opening and closing times from 10 to 20 ms. The V3/3P is operated by a solenoid valve (Bürkert 5/2) and a pneumatic actuator (Prisma). In addition, a hand-operated ball valve (valve V3/3H) is positioned next to the electro-pneumatically actuated ball valve.

The test procedure is as follows. The steady state flow conditions (in advance of a dynamic test) are controlled by a set pressure in the upstream end tank and by a set opening of the downstream end control needle valve (valve V3/3C in Fig. 1). The water level in the upstream end pressurized tank can be adjusted. From initial steady flow conditions (flow, no-flow), a transient event is initiated by some valve manipulations.

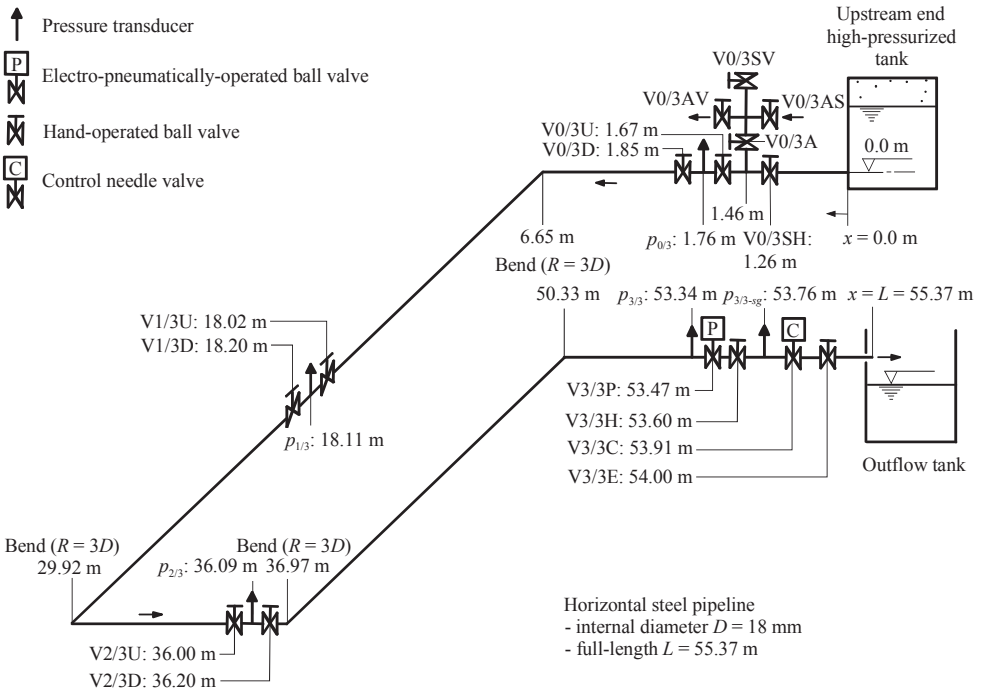

Figure 1: *Layout of small-scale pipeline apparatus, [14]*

Four dynamic pressure transducers are positioned within the valve units along the pipeline including the end points (see Fig. 1). Pressures $p_{0/3}$, $p_{1/3}$, $p_{2/3}$ and $p_{3/3}$ are measured with Dytran 2300V4 high frequency piezoelectric absolute pressure transducers (pressure range: from 0 to 6.9 MPa; resonant frequency: 50 kHz; acceleration compensated; discharge time constant: 10 seconds (fixed); uncertainty U_x = ±1 % for Δp duration of 100 ms). The uncertainty in a measured quantity (U_x) is expressed as a sum of bias and precision errors. All four piezoelectric transducers were flush mounted to the inner pipe wall. For evaluation of the initial conditions in the system, two Endress+Hauser PMP131 strain-gauge pressure transducers are positioned at the upstream end pressurized tank and at the control valve V3/3C (pressure range: from 0 to 1 MPa; U_x = ±0.5%). The datum level for all pressures measured in the pipeline and at the tank is at the top of the horizontal steel pipe (elevation 0.0 m in Fig. 1). The downstream end valves V3/3P and V3/3H are equipped with Positek P500.90BL fast-response displacement sensors (measurement range: from 0 to 90°; frequency response: 10 kHz; U_x = ±0.5°). The sensors measure the change of the

valve angle during valve closing and opening events. Figure 2 shows the layout of the downstream end valve unit with instruments including two pressure transducers and two valve displacement sensors. The initial discharge (Q_0) and, consequently, the initial flow velocity (V_0) are measured with different methods (U_x = ±1%). For initial flow velocities larger than 0.3 m/s, an electromagnetic flow meter Khrone OPTIFLUX 4000F IFC 300C is used. Smaller steady state velocities are estimated from the Joukowsky pressure head rise or drop resulting from the rapid valve action. The water temperature is continuously monitored with the thermometer (U_x = ±0.5° C) installed in the outflow tank. The water hammer wave speed was determined as a = 1340 m/s (U_x = ±1%). Column separation experiments presented in this paper have shown a good repeatability of the magnitude and timing of the main pressure pulses.

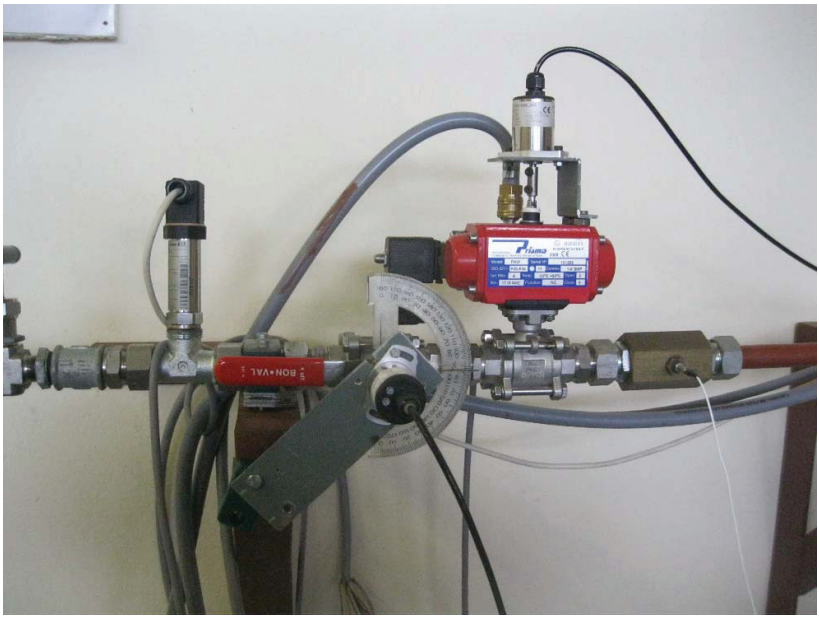

Figure 2: *Layout of downstream end valve unit with instruments.*

4 COMPARISONS OF COMPUTED AND TEST RESULTS

This section presents numerical and experimental results from two distinct column separation runs including active and passive column separation cases [4]. Numerical results from the discrete gas cavity model with consideration of (1) quasi-steady friction (DGCM+QSF) and (2) unsteady skin friction (DGCM+CBM) [10] are compared with results of measurements performed in the laboratory pipeline apparatus – see Fig. 1. The two runs were carried out for a rapid closure of the hand-operated ball valve positioned at the downstream end of the horizontal pipe (valve V3/3H in Fig. 1). The sampling frequency for each dynamically measured quantity was f_s = 2000 Hz. Pressures measured at the end points (positions 0/3 and 3/3) and at the two equidistant positions along the pipeline (positions 1/3 and 2/3) are compared with computational results as

piezometric heads (heads) with a datum level at the top of the horizontal pipe (elevation 0.0 m in Fig. 1). The number of reaches for all computational runs were N = 108.

4.1 Active column separation case

The active column separation case represents a transient event with a maximum head rise larger than the Joukowsky head rise ($\Delta H_J = (a/g)V_0$), [4]. The initial flow velocity and the upstream end reservoir head were V_0 = 0.44 m/s and H_{HPT} = 30.5 m, respectively. Numerical and experimental results for this case are depicted in Figs. 3 and 4. The effective valve closure time of 0.025 s was much less than the wave reflection time $2L/a$ of 0.08 seconds. A rapid valve closure generates a column separation event with limited cavitation. The valve closure first induced Joukowsky head rise at the valve (ΔH_J = 60 m) and subsequently in time t = 0.09 s column separation at the valve. The negative wave travels along the pipeline and drops the head to the vapour pressure head at all measured positions along the pipeline. The maximum measured head at the valve $H_{3/3max}$ = 125 m occurs as a short-duration pressure pulse after the first cavity collapses. The duration of the maximum measured head is very short (0.015 s).

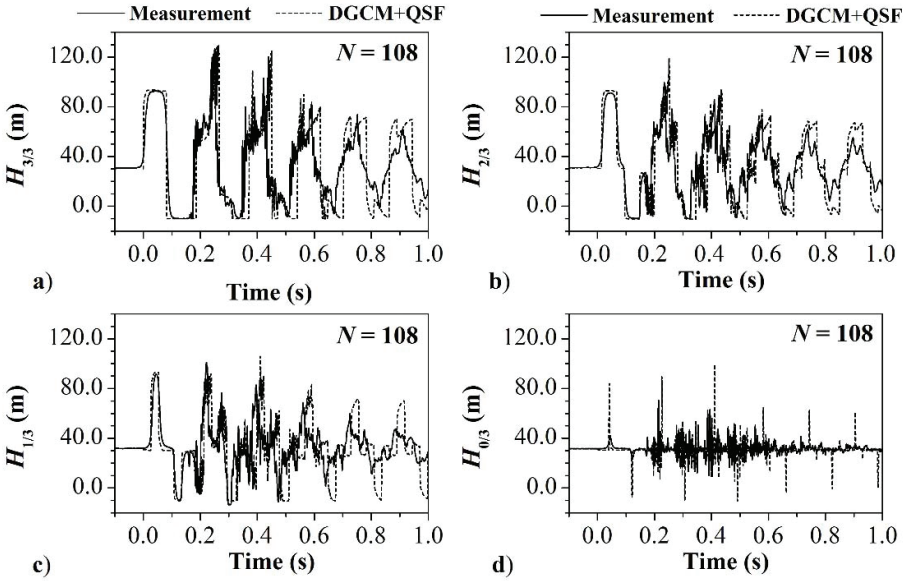

Figure 3: *Comparisons of measured and DGCM+QSF-calculated heads at the end points ($H_{0/3}$ and $H_{3/3}$) and at the two equidistant positions along the pipeline ($H_{1/3}$ and $H_{2/3}$); V_0 = 0.44 m/s.*

The maximum head obtained by DGCM+QSF (Fig. 3) is slightly higher than the measured one; it is $H_{3/3max}$ = 128 m. In contrast, the maximum computed head predicted by DGCM+CBM (Fig. 4) is slightly lower $H_{3/3max}$ = 110 m. The difference between the measured and calculated heads is due to the slightly different timing of the cavity collapse. The DGCM+QSF model gives good agreement with measured results for the first two pressure pulses. After that, a phase shift is obvious as well as lesser

attenuation of pressure traces (Fig. 3). This is not the case for DGCM+CBM results. The results agree well with the measured results during the whole period of observation (Fig. 4).

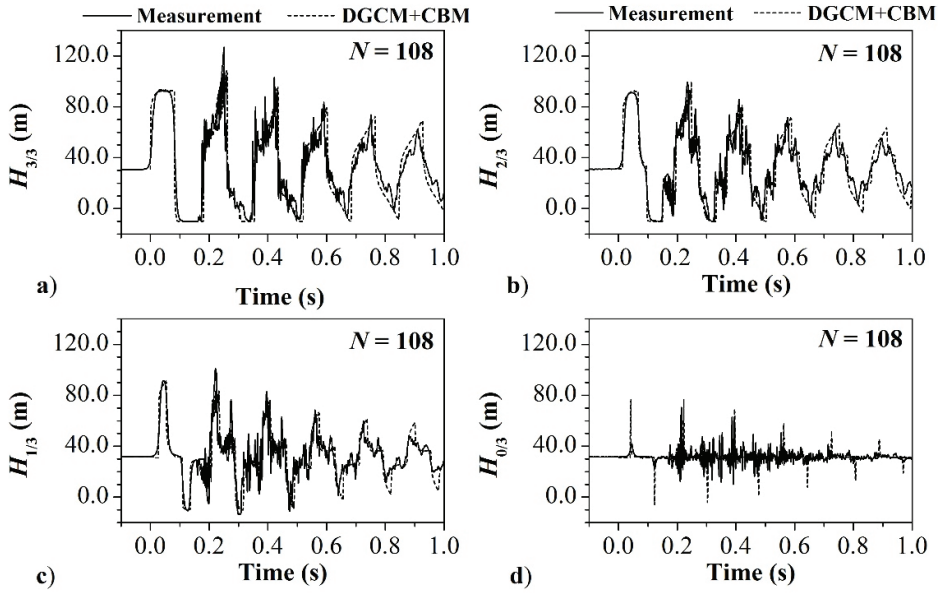

***Figure 4**: Comparisons of measured and DGCM+CBM-calculated heads at the end points ($H_{0/3}$ and $H_{3/3}$) and at the two equidistant positions along the pipeline ($H_{1/3}$ and $H_{2/3}$); V_0 = 0.44 m/s.*

4.2 Passive column separation case

The passive column separation case is a transient event with a maximum head rise equal to the Joukowsky head rise (ΔH_J), [4]. The initial flow velocity and the upstream end reservoir head were V_0 = 2.19 m/s and H_{HPT} = 48 m, respectively. Numerical and experimental results for this case are shown in Figs. 5 and 6. The effective valve closure time of 0.020 s was much less than the wave reflection time 2L/a of 0.08 seconds, and it was about 50% of the total closure time. A rapid valve closure generates a column separation event with severe cavitation. The valve closure first induced a Joukowsky head rise at the valve (ΔH_J = 300 m excluding friction effect and ΔH_J = 315 m with friction) and subsequently, in time t = 0.09 s, severe column separation at the valve. The negative wave travels along the pipeline and drops the head to the vapour pressure head at all measured positions along the pipeline. The maximum measured head at the valve $H_{3/3max}$ = 295 m after the first cavity collapsed is less than the Joukowsky head H_J = 340 m. Pressure histories along the pipeline (Figs. 5b to 5c and 6b to 6c, respectively) enable accurate tracing of distributed vaporous cavitation zones and intermediate cavities. For this case the maximum measured head at the valve $H_{3/3max}$ = 340 m occurs as the Joukowsky water hammer head at the valve just before the first liquid column separation.

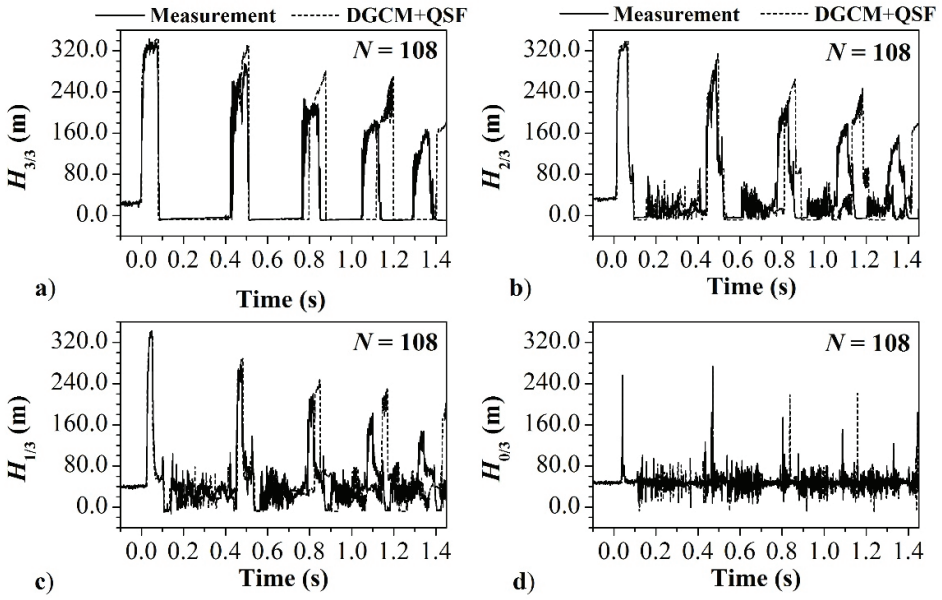

Figure 5: *Comparisons of measured and DGCM+QSF-calculated heads at the end points ($H_{0/3}$ and $H_{3/3}$) and at the two equidistant positions along the pipeline ($H_{1/3}$ and $H_{2/3}$); V_0 = 2.19 m/s.*

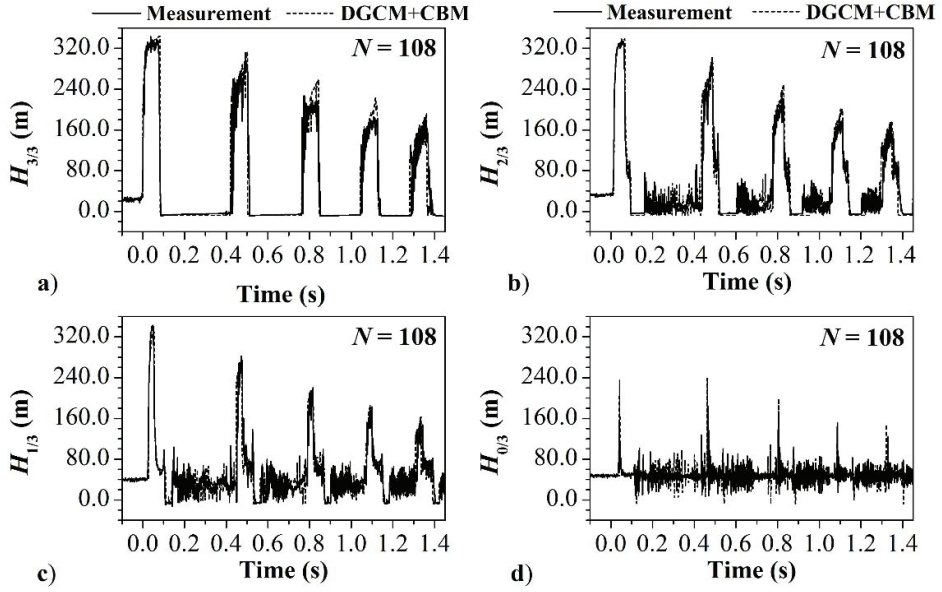

Figure 6*: Comparisons of measured and DGCM+CBM-calculated heads at the end points ($H_{0/3}$ and $H_{3/3}$) and at the two equidistant positions along the pipeline ($H_{1/3}$ and $H_{2/3}$); V_0 = 2.19 m/s.*

For the passive column separation case, the maximum measured and calculated pressure heads are in excellent agreement; see Figs. 5a and 6a, respectively. Again the DGCM+QSF model gives good agreement with the measured results for the first two bulk pressure pulses. After that, there are significant differences between the measured and calculated results (Fig. 5). In contrast, the DGCM+CBM results agree well with measured ones during the whole period of observation (Fig. 6).

5 CONCLUSIONS

Numerical results are compared with the results of the measurements given for the closure of the downstream end ball valve in the pipeline apparatus. Pressures measured at the end points (positions 0/3 and 3/3 in Fig. 1) and at the two equidistant positions along the pipeline (positions 1/3 and 2/3) are compared with computational results as piezometric heads (heads). Two distinct column separation runs include active and passive column separation cases. The DGCM model using a quasi-steady friction approach (DGCM+QSF) gives good agreement with the measured results for the first two pressure pulses. After that, there are significant differences between the measured and calculated results. In contrast, the advanced discrete gas cavity model with the consideration of unsteady skin friction (DGCM+CBM) performs well throughout the period of observation. Therefore, the discrete gas cavity model using the convolution-based unsteady friction term is recommended for engineering practice.

References

[1] **E.B. Wylie, V.L. Streeter:** *Fluid Transients in Systems*, Prentice Hall, 1993

[2] **M.H. Chaudhry:** *Applied Hydraulic Transients,* Springer, 2014

[3] **A. Bergant, A.S. Tijsseling, J.P. Vítkovský, D.I.C. Covas, A.R. Simpson, M.F. Lambert:** *Parameters affecting water-hammer wave attenuation, shape and timing. Part 1: Mathematical tools and Part 2: Case studies*, Journal of Hydraulic Research, IAHR, Vol. 46, Iss. 3, Part 1, p.p. 373 – 381 and Part 2, p.p. 382 – 391, 2008

[4] **A. Bergant, A.R. Simpson:** *Pipeline column separation flow regimes*, Journal of Hydraulic Engineering, ASCE, Vol. 125, Iss. 8, p.p. 835 – 848, 1999

[5] **A. E. Vardy, J.M.B. Brown:** *Evaluation of unsteady wall shear stress by Zielke's method*, Journal of Hydraulic Engineering, ASCE, Vol. 136, Iss. 7, p.p. 453 – 456, 2010

[6] **A. S. Tijsseling:** *Fluid-structure interaction in liquid-filled pipe systems: a review*, Journal of Fluids and Structures, Vol. 10, Iss. 2, p.p. 109 – 146, 1996

[7] **D. Covas, I. Stoianov, F.J. Mano, H. Ramos, N. Graham, Č. Maksimović:** *The dynamic effect of pipe-wall viscoelasticity in hydraulic transients. Part I - experimental analysis and creep characterisation and Part II - model development, calibration and verification*, Journal of Hydraulic Research, IAHR, Part - I, Vol. 42, Iss. 5, p.p. 516 – 530 and Part - II, Vol. 43, Iss. 1, p.p. 56 – 70, 2004 and 2005

[8] **A. Malekpour, W.B. Karney:** *Profile-induced column separation and rejoining during pipeline filling,* Journal of Hydraulic Engineering, ASCE, Vol. 140, Iss. 11, p.p. 04014054–1 – 12, 2014

[9] **U. Karadžić, V. Bulatović, A. Bergant:** *Valve-induced water hammer and column separation in a pipeline apparatus*, Strojniški Vestnik – Journal of Mechanical Engineering, Vol.60, Iss. 11, p.p. 742 – 754, 2014

[10] **A. Bergant, U. Karadžić, J.P. Vítkovský, I. Vušanović, A.R. Simpson:** *A discrete gas cavity model that considers the frictional effects of unsteady pipe flow*, Strojniški vestnik - Journal of Mechanical Engineering, Vol. 51, Iss. 11, p.p. 692 – 710, 2005

[11] **A. Bergant, A.R. Simpson, J.P. Vítkovský:** *Developments in unsteady pipe flow friction modelling*, Journal of Hydraulic Research, IAHR, Vol. 39, Iss. 3, p.p. 249 – 257, 2001

[12] **J. P. Vítkovský, M. Stephens, A. Bergant, M.F. Lambert, A.R. Simpson:** *Efficient and accurate calculations of Zielke and Vardy-Brown unsteady friction in pipe transients*, 9th International Conference on Pressure Surges, BHR Group, Chester, England, 2004

[13] **W. Zielke:** *Frequency-dependent friction in transient pipe flow,* Journal of Basic Engineering, ASME, Vol. 90, Iss. 1, p.p. 109 – 115, 1968

[14] **U. Karadžić, F. Strunjaš, A. Bergant, R. Mavrič, S. Buckstein:** *Developments in pipeline filling and emptying experimentation in a laboratory pipeline apparatus*, 6th IAHR Meeting of the Working Group Cavitation and Dynamic Problems in Hydraulic Machinery and Systems, Ljubljana, Slovenia, 2015

Nomenclature

(Symbols)	(Symbol meaning)
A	pipe area
a	water hammer wave speed
D	pipe diameter, diameter
f	friction factor
f_s	sampling frequency
g	gravitational acceleration
H	piezometric head, head
L	length
N	number of reaches; number of y_k components
p	pressure
Q	discharge
t	time
U_x	uncertainty in a measured quantity
V	flow velocity
x	distance along the pipe

y_k	component of the weighting function in Eq. 2.6
α	void fraction
ν	kinematic viscosity
ΔH	head rise
$\forall$	volume
(Subscripts)	(Subscripts meaning)
g	gas
HPT	high-pressurized tank, reservoir
in	inflow
J	Joukowsky head
max	maximum
out	outflow
q	quasi-steady part
u	unsteady part
0	initial conditions
(Superscripts)	(Superscripts meaning)
*	absolute pressure
(Abbreviations)	(Abbreviations meaning)
CBM	Convolution-Based Model
DGCM	Discrete Gas Cavity Model
FSI	Fluid-Structure Interaction
MOC	Method Of Characteristics
QSF	Quasi-Steady Friction

Acknowledgments

The authors wish to thank Slovenian Research Agency (ARRS) and Ministry of Science, Montenegro (MSM) for their support for this research conducted through the projects BI-ME/14-15-016 (ARRS, MSM) and L2-5491 (ARRS).

Journal of Energy Technology

JET Volume 8 (2015) p.p. 43-58
Issue 2, October 2015
Typology of article 1.01
www.fe.um.si/en/jet.html

INTEGER PROGRAMMING AND GRÖBNER BASES

CELOŠTEVILSKO PROGRAMIRANJE IN GRÖBNERJEVE BAZE

Brigita Ferčec[1], Matej Mencinger[R]

Keywords: Integer linear programming, polynomial rings, Gröbner bases, nonlinear polynomial systems of equations

Abstract

An approach to solve the integer linear programming problem (IP) using the Gröbner bases theory is presented. We consider the basics of commutative algebra on polynomial rings and their ideals and the multidivision algorithm. Gröbner bases were introduced to solve nonlinear polynomial systems of equations; therefore, we first present the generalization of the Gauss elimination method. In order to solve a general IP a special ideal depending on the coefficients of the system and number of constraints in the IP has to be constructed. Finally, a Gröbner basis of this ideal, which yields the solution to IP, must be sought.

Povzetek

V članku je podan pristop k reševanju celoštevilskega linearnega programiranja (IP) z uporabo teorije Gröbnerjevih baz. Obravnavamo osnovne elemente komutativne algebre na polinomskih kolobarjih, njihove ideale in algoritem multi-deljenja. Gröbnerjeve baze so bile vpeljane za reševanje nelinearnih polinomskih sistemov enačb, zato je v članku najprej predstavljen primer posplošitve Gaussove eliminacijske metode. Pri reševanju splošnega IP konstruiramo poseben ideal, ki je odvisen od koeficientov sistema in števila enačb v IP. Končno rešitev dobimo s pomočjo Gröbnerjeve baze tega ideala.

[R] Corresponding author: Integer programming and Gröbner bases, Matej Mencinger, Tel.: +386 2 229 4321, Mailing address: University of Maribor, Faculty of Civil Engineering, Transportation Engineering and Architecture, Smetanova ulica 17, 2000 Maribor, Slovenia, E-mail address: matej.mencinger@um.si

[1]Faculty of Energy Technology, Hočevarjev trg 1, 8270 Krško

1 INTRODUCTION

Many modern computer programs, such as Mathematica, Matlab and others, enable solving the problem of integer (linear) programming (IP). There are several algorithms to solve the problem of IP; one of the most known and commonly used is the so called 'Branch and bound algorithm'. In this paper, we consider another aspect of solving this problem, which is based on the theory of Gröbner bases, which is the basis of the ideal of a polynomial ring in a similar sense as the vector space $(\mathbb{R}^n, +)$, which has a basis consisting of n linearly independent vectors (1,0,0,…,0), (0,1,0,…,0), ..., (0,0,0,…,1). These n vectors are called a standard basis of $(\mathbb{R}^n, +)$ and in a similar sense theGröbner basis is called a standard basis of the given ideal.

Turning now to the IP, where there are more equations and variables, and a cost function to be optimized, and taking into account that the main objects of the polynomials of several variables are monomials, we can use the fact that the exponent of each monomial is actually a vector. As we will see later, this vector is naturally related to independent variables of IP that are (basically positive) integers.

There are many different ways of examining the theory of Gröbner bases. In the context of classical algebra, the natural point of view is as follows.

We consider polynomials in variables $x_1, \dots, x_n$ with coefficients a_α of a field k. We call $x^\alpha = x_1^{\alpha_1} \cdots x_n^{\alpha_n}$ a *monomial*, $a_\alpha \in k$ a *coefficient* and $a_\alpha x_1^{\alpha_1} \cdots x_n^{\alpha_n}$ a *term*, and $\alpha = (\alpha_1, \dots, \alpha_n)$ a *multi-index*. The set of all polynomials in variables $x_1, \dots, x_n$ with coefficient in k is denoted by $k[x_1, \dots, x_n]$. With the usual operations of addition and multiplication, $k[x_1, \dots, x_n]$ is a commutative ring (i.e. the multiplication in the ring is symmetric). We call $\alpha = \alpha_1 + \cdots + \alpha_n$ the full degree of a monomial x^α. The degree of a polynomial f, denoted by $\deg(f)$, is the maximum degree of a monomial of f. For any natural number n, the space

$$k^n = \{(a_1, \dots, a_n) : a_1, \dots, a_n \in k\}$$

is called n −dimensional *affine space*. The set of polynomials $f_1, \dots, f_s$ is naturally associated with a system of equations

$$\begin{aligned} f_1(x_1, \dots, x_n) &= 0, \\ &\vdots \\ f_s(x_1, \dots, x_n) &= 0. \end{aligned} \tag{1.1}$$

The set of all solutions to the above system can be defined as the *affine variety*, $\boldsymbol{V}$, determined by polymomials $f_1, \dots, f_s$:

$$\boldsymbol{V}(f_1, \dots, f_s) = \{(a_1, \dots, a_n) \in k^n : f_j(a_1, \dots, a_n) = 0 \; for \; 1 \le j \le s\}.$$

It is clear that there are many families of polynomials defining the same variety. For example, if $f_1 = x - y$, $f_2 = y - 1$ and $g_1 = (y - x)^3$, $g_2 = y^2 - 2y + 1$, then $\boldsymbol{V}\langle f_1, f_2\rangle = \boldsymbol{V}\langle g_1, g_2\rangle$. To understand the concept of an affine variety better we need the notion of an ideal.

An *ideal* in the polynomial ring $k[x_1, \dots, x_n]$ is a subset I of $k[x_1, \dots, x_n]$ satisfying

i. if $f, g \in I$ then $f + g \in I$ and
ii. if $f \in I$ and $h \in k[x_1, \dots, x_n]$, then $hf \in I$.

Let $f_1, \dots, f_s$ be polynomials of $k[x_1, \dots, x_n]$. We denote

$$\langle f_1, \dots, f_s \rangle = \left\{ \sum_{j=1}^{s} h_j f_j \mid h_1, \dots, h_s \in k[x_1, \dots, x_n] \right\}.$$

It is easily seen that $\langle f_1, \dots, f_s \rangle$ is an ideal in $k[x_1, \dots, x_n]$. Polynomials $f_1, \dots, f_s$ are called *generators* of this ideal. Ideal $I \subset k[x_1, \dots, x_n]$ is *finitely generated* if there exist polynomials $\langle f_1, \dots, f_s \rangle \in k[x_1, \dots, x_n]$ such that $I = \langle f_1, \dots, f_s \rangle$, and the set $\{f_1, \dots, f_s\}$ is called a *basis* of I.

From the definition of an affine variety, we see that to find an affine variety $\boldsymbol{V}(f_1, \dots, f_s) \subset k^n$ is equivalently as to find the set of solutions of system (1.1). This is a problem that frequently arises in studies of various phenomena in physical, technical and other sciences. In particular, in order to study the qualitative behaviour of dynamics system

$$\dot{x}_1 = f_1(x_1, x_2, \dots, x_n) = 0, \dots, \dot{x}_s = f_s(x_1, x_2, \dots, x_n)$$

we first have to determine singular points of the system, which are the points where all polynomials $f_1, \dots, f_s$ vanish. Thus, we again arrive at a problem of the form (1.1), [6,7,10].

The problem of finding solutions of system (1.1) is very difficult. It can happen that system (1.1) has infinitely many solutions, which means that it is impossible to find (all) solutions numerically. Even if system (1.1) has a finite number of solutions it is still very difficult and often impossible to find all of them numerically without applying methods of computational algebra.

In the next section, we describe the concept of Gröbner bases, which is closely related to the multivariable division algorithm. We consider the main properties of Gröbner bases and connect them to the solution of system (1.1). In the third section, we study the main topic of this paper, the integer programming problem (IP) via the theory of Gröbner bases. We demonstrate the application of the theory of Gröbner bases theory to IP on two examples. In the first example, we consider a case of IP without a cost function (i.e. just a problem to find integer solutions to $A\vec{x} = \vec{b}$), while in the second example we search for the solutions to a general IP (with a given cost function).

2 GRÖBNER BASIS AND NONLINEAR SYSTEMS OF EQUATIONS

Until the mid-1960s, when Bruno Buchberger, [2], invented the theory of Gröbner bases, no method for solving a general (nonlinear polynomial) system (1.1) was known. What is nowadays called Buchberger's algorithm (and Gröbner basis) is actually the cornerstone of modern computational algebra. In this section, we first briefly describe the notion of a Gröbner basis, which will be used to obtain the variety of an ideal generated by polynomials $f_1, \dots, f_s$, i.e. to obtain the solution of system (1.1). Since a Gröbner basis of I depends on a term ordering on monomials of $k[x_1, \dots, x_n]$, we define monomial (term) order.

A *monomial order* $<$ on $k[x_1, \dots, x_n]$ is a total order $<$ on $\mathbb{N}_0^n$ with the following two properties:

(i) any nonempty subset of monomials has a least element (under <),

(ii) if $x^\alpha < x^\beta$ then $x^\alpha x^\gamma < x^\beta x^\gamma$ for every monomial x^γ.

The most common monomial ordering is shown in the following example.

Let us consider $x_1^2x_2^8x_3^{50}, x_1^3x_2^2x_3^5, x_1^2x_2^9x_3^4 \in \mathbb{R}[x_1, x_2, x_3]$ and say, x_1 is 'more important' than x_2 (and x_3) and x_2 is 'more important' than x_3. Then:

$$x_1^3x_2^2x_3^5 > x_1^2x_2^9x_3^4 > x_1^2x_2^8x_3^{50}.$$

This monomial order is called a *lexicographic (monomial) order*. More precisely, $x^\alpha < x^\beta$ if and only if the first coordinates $\alpha_i$and β_i in α and β from left, which are different, satisfy $\alpha_i < \beta_i$. There are many other standard monomial orders, like (graded) reverse lexicographic, (graded) reverse lexicographic, etc. [4]. To avoid the, we can emphasize the name of the monomial order. For example $<_{lex}$ stands for the lexicographic order.

As soon as the monomial order is chosen, we can speak of the so-called *leading monomial* (LM), *leading term* (LT) and *leading coefficient* (LC) of the polynomial. The leading term is defined with the largest (with respect to fixed order) monomial.

For example, if $f = -x_1^2x_2^8x_3^{50} + 2x_1^3x_2^2x_3^5 + 3x_1^2x_2^9x_3^4$ and the order is lexicographic with $x_1 > x_2 > x_3$, the leading term of f is $LT(f) = 2x_1^3x_2^2x_3^5$, whilst the leading coefficient is $LC(f) = 2$ and the leading monomial $LM(f) = x_1^3x_2^2x_3^5$.

Finally, note that any vector $\vec{c} \in \mathbb{R}^n$ defines an monomial order $<_{\vec{c}}$ in $\mathbb{R}[x_1, \dots, x_n]$ in the following way:

$$\vec{x}^{\vec{\alpha}} <_{\vec{c}} \vec{x}^{\vec{\beta}} \Leftrightarrow \begin{cases} \vec{c} \cdot \vec{\alpha} < \vec{c} \cdot \vec{\beta} & or \\ \vec{c} \cdot \vec{\alpha} = \vec{c} \cdot \vec{\beta} \quad and\ \vec{\alpha} <_{lex} \vec{\beta}, \end{cases}$$

where $\vec{c} \cdot \vec{\alpha}$ stands for the standard dot product $\vec{c} \cdot \vec{\alpha} = \sum_i c_i\alpha_i$. This monomial term order $<_{\vec{c}}$ defined by vector $\vec{c}$ is usually called *weighted* (monomial) *order*.

For example, if $\vec{c} = (1,5,10)$, we have $x_1^5x_2^1x_3^2 <_{\vec{c}} x_1^1x_2^0x_3^3$ since $\vec{c} \cdot \vec{\alpha} = (1,5,10) \cdot (5,1,2) = 30$ and $\vec{c} \cdot \vec{\beta} = (1,5,10) \cdot (1,0,3) = 31$ (and $30 < 31$). Note, that for $<_{\vec{c}}$ the leading term of $g = 2x_1^5x_2^1x_3^2 - 5x_1^1x_2^0x_3^3$ is $LT(g) = -5x_1^1x_3^3$ while for $<_{lex}$ the leading term of (the same) g is $LT(g) = 2x_1^5x_2^1x_3^2$.

Now, we describe the procedure of multi-division of a polynomial by an ordered set of polynomials, that is to divide $f \in k[x_1, \dots, x_n]$ by an ordered set $F = \{f_1, \dots, f_s\}$, which means to express f in the form

$$f = q_1f_1 + q_2f_2 + \cdots + q_sf_s + r, \tag{1.2}$$

where the quotients $q_1, \dots, q_s$ and the reminder r are polynomials of $k[x_1, \dots, x_n]$, and either $r = 0$ or $\deg(r) < \deg(f)$. In this case (1.2) means that f is reduced to r modulo F, and we write

$$f \xrightarrow{F} r.$$

The process of multi-division depends on the monomial order and the order of the polynomials in the set $F = \{f_1, \dots, f_s,\}$. So, we have to fix the monomial order first to perform the multidivision. For the precise introduction to multivariable division algorithm see e.g. Adams & Luostaunau (1994), Cox et al. (2007), and Romanovski & Shafer (2009). We demonstrate the division process by the following example.

Let us divide $f = x^2y + xy^2 + y^2$ by the ordered set of polynomials $F = \{f_1, f_2\} = \{xy - 1, y^2 - 1\}$ using lexicographic order with $x > y$.

$$\begin{array}{rl|l}
q_1: & x+y & \\
q_2: & 1 & r \\
f_1: xy-1 & \sqrt{x^2y+xy^2+y^2} & \\
f_2: y^2-1 & & \\
 & \underline{x^2y - x} & \\
 & \quad xy^2+x+y^2 & \\
 & \quad \underline{xy^2 - y} & \\
 & \quad\quad x+y^2+y & \\
 & \quad\quad \underline{y^2+y} \quad \to \quad x & \\
 & \quad\quad\quad y^2-1 & \\
 & \quad\quad\quad \underline{y+1} & \\
 & \quad\quad\quad\quad \underline{1} \quad \to \quad x+y & \\
 & \quad\quad\quad\quad 0 \quad \to \quad x+y+1 &
\end{array}$$

Figure 1: *The scheme of multivariable division procedure*

On the first step, the leading term $LT(f_1) = xy$ divides the leading term $LT(f) = x^2y$. Thus, we divide x^2y by xy, leaving x and then subtract $x \cdot f_1$ from f. Next, we repeat the same process on $x\,y^2 + x + y^2$. We divide f by $LT(f_1) = xy$ again. Note that neither $LT(f_1) = xy$ nor $LT(f_2) = y^2$ divides $LT(x + y^2 + y) = x$. However, $x + y^2 + y$ is not the remainder since $LT(f_2)$ divides y^2. Thus, if we move x to the remainder column, we can continue with the process. If we can divide by $LT(f_1)$ or $LT(f_2)$, we proceed as usual, otherwise, we move the leading term of the intermediate dividend (the polynomial under the radical sign) to the remainder column. We continue dividing in such a way. Now the polynomial under the radical is $y^2 + y$. It is not divisible by $LT(f_1)$ but we can divide it by $LT(f_2)$ yielding 1 and the subtract $1 \cdot y^2$ from $y^2 + y$. The obtained polynomial under the radical is $y + 1$ and neither $LT(f_1)$ nor $LT(f_2)$ is divisible by $LT(y + 1) = y$. Therefore, we move y to the remainder column and obtain 1, which is also moved to the remainder column. Thus, the remainder is $x + y + 1$ and this concludes the example. Thus, we can write f in the form

$$f = x^2y + xy^2 + y^2 = (x + y) \cdot (xy - 1) + 1 \cdot (y^2 - 1) + x + y + 1.$$

In contrast, if we change the order of polynomials f_1 and f_2 in F, i.e. if we divide f by the ordered set $F = \{f_2, f_1\}$, we obtain

$$f = x^2y + xy^2 + y^2 = x \cdot (xy - 1) + (x + 1) \cdot (y^2 - 1) + 2x + 1.$$

Obviously, this multivariable division is very sensitive on the order of f_1, f_2. The order affects the *multi-quotients* q_1, q_2, as well as the *remainder* r. Dividing the polynomial f with the (ordered) set $F = \{f_1, f_2\}$, one can simply write: $f = \{\{q_1, q_2\}, r\}$ instead of $f = q_1f_1 + q_2f_2 + r$. Using this notation, in the first case, we have $f = \{\{x + y, 1\}, x + y + 1\}$ and in the second case we have $f = \{\{x, x + 1\}, 2x + 1\}$. Figure 2 shows the last results obtained by the MATHEMATICA computer algebra system. The multi-quotients and the remainder are also changed if we use another monomial order.

```
In[1]:= PolynomialReduce[x^2 y + x y^2 + y^2, {x y - 1, y^2 - 1}, {x, y}]

Out[1]= {{x + y, 1}, 1 + x + y}

In[2]:= PolynomialReduce[x^2 y + x y^2 + y^2, {y^2 - 1, x y - 1}, {x, y}]

Out[2]= {{1 + x, x}, 1 + 2 x}
```

Figure 2: *Results obtained by MATHEMATICA for the case above*

Now, we present the basic definitions and properties of Gröbner bases. For any ideal, $\boldsymbol{I}$ we define $\langle \boldsymbol{LT(I)} \rangle = \langle \boldsymbol{LT(f)}: \boldsymbol{f} \in \boldsymbol{I} \setminus \{\boldsymbol{0}\} \rangle = \langle \boldsymbol{LM(f)}: \boldsymbol{f} \in \boldsymbol{I} \setminus \{\boldsymbol{0}\} \rangle$. A Gröbner basis of an ideal $\boldsymbol{I} \subset \boldsymbol{k}[\boldsymbol{x_1}, , \dots, \boldsymbol{x_n}]$ is a finite subset $\boldsymbol{G} = \{\boldsymbol{g_1}, \dots, \boldsymbol{g_t}\}$ of $\boldsymbol{I}$ such that

$$\langle LT(I) \rangle = \langle LT(g_1), \dots, LT(g_t) \rangle.$$

It is a special generating set for ideal $\langle f_1, \dots, f_n \rangle$ for which the multivariable division algorithm for a given f returns the remainder $r = 0$ if and only if $f \in \langle g_1, \dots, g_t \rangle$,[4].
Using a Gröbner basis, we obtain the uniqueness of the remainder, which was not assured when we divided by an arbitrary set of polynomials, [2].
We now describe an algorithm for computing a Gröbner basis of a polynomial ring. Let f, g be from $k[x_1, \dots, x_n]$ with $LT(f) = ax^\alpha$ and $LT(g) = bx^\beta$. The *least common multiple* of x^α and x^β, denoted $LCM(x^\alpha, x^\beta)$, is the monomial $x^\gamma = x_1^{\gamma_1} \cdots x_n^{\gamma_n}$ such that $\gamma_j = \max(\alpha_j, \beta_j)$, $1 \leq j \leq n$. The so-called S −polynomial of f and g is

$$S_{f,g} = \frac{x^\gamma}{LT(f)} \cdot f - \frac{x^\gamma}{LT(g)} \cdot g.$$

Buchcberger's basic observation was the following criterion, [2]. Let I be a nonzero ideal in $k[x_1, \dots, x_n]$ and let $<$ be a fixed monomial order on $k[x_1, \dots, x_n]$. Then, $G = \{g_1, g_2, \dots, g_t\}$ is a Gröbner basis for I with respect to $<$ if and only if for all $i \neq j$

$$S_{g_i,\ g_j} \xrightarrow{G} 0.$$

This criterion is the essence of the famous *Buchberger's algorithm*, which produces a Gröbner basis for the nonzero ideal $I = \langle f_1, \dots, f_s \rangle$. Buchberger's algorithm is shown below, [11].

Buchberger's Algorithm

Input: A set of polynomials $\{f_1, \dots, f_s\} \in k[x_1, \dots, x_n] \backslash \{0\}$.
Output: A Gröbner basis G of the ideal $\langle f_1, \dots, f_s \rangle$.
Procedure: $G := \{f_1, \dots, f_s\}$.
Step 1. For each pair $g_i, g_j \in G, i \neq j$, compute the S −polynomial S_{g_i,g_j} and compute the remainder $r_{i,j}$ of division S_{g_i,g_j} by the set G.
Step 2. Check if all $r_{i,j}$ are equal to zero . If "yes", then G is a Gröbner basis, otherwise add all nonzero $r_{i,j}$ to G and return to step 1.

It is proved in [2] that the algorithm terminates and returns a Gröbner basis of the ideal $I = \langle f_1, f_2, \dots, f_n \rangle$.
Nowadays, all well-known computer algebra systems (MATHEMATICA, SINGULAR, MAPLE, REDUCE, and others) have routines to compute Gröbner bases.
Even if a monomial order is fixed, an imprecision in the computation of a Gröbner basis arises because the division algorithm can produce different remainders for different orderings of polynomials in the set of divisors. Thus the output of Buchberger's Algorithms is not unique; neither is it minimal (in the sense that it contains more polynomials then necessary).
A Gröbner basis $G = \{g_1, \dots, g_m\}$ is called minimal if, for all $i, j \in \{1, \dots, m\}$, $LC(g_i) = 1$ and for $j \neq i$, $LM(g_i)$ does not divide $LM(g_j)$. Every nonzero polynomial ideal has a minimal Gröbner basis, [4]. If no term of g_i is divisible by any $LT(g_j)$ for $j \neq i$ then the Gröbner basis is called reduced and if we fix a monomial order then every nonzero ideal $I \subset k[x_1, \dots, x_n]$ has a unique reduced Gröbner basis with respect to this order.

In Figures 3 and 4, the Gröbner basis of the ideal $\langle -x^3 + y, x^2 y - y^2 \rangle$ with respect to lexicographic monomial order with $x > y$ is computed in systems MATHEMATICA and SINGULAR, [9], respectively. We see that in both cases the result is $\{y^3 - y^2, xy^2 - y^2, x^2 y - y^2, x^3 - y\}$.

```
In[6]:= GroebnerBasis[{-x^3 + y, x^2 y - y^2}, {x, y}]
Out[6]= {-y^2 + y^3, -y^2 + x y^2, x^2 y - y^2, x^3 - y}
```

Figure 3: *Output of Gröbner basis in system MATHEMATICA*

```
                     SINGULAR                                 /
 A Computer Algebra System for Polynomial Computations       /   version 3-1-
                                                           0<
 by: W. Decker, G.-M. Greuel, G. Pfister, H. Schoenemann     \   Jan 2012
FB Mathematik der Universitaet, D-67653 Kaiserslautern        \
> ring r1=0, (x,y),lp;
> poly f1=-x3+y;
> poly f2=x2*y-y2;
> ideal I=f1,f2;
> ideal G=groebner(I);
> G;
G[1]=y3-y2
G[2]=xy2-y2
G[3]=x2y-y2
G[4]=x3-y
>
```

Figure 4: *Output of Gröbner basis in system SINGULAR*

A reason to use more special systems than MATHEMATICA offers is to compute the Gröbner basis with respect to some special monomial order. In Figure 5 we compute the Gröbner basis of $\langle -x^3+y, x^2y-y^2\rangle$ using SINGULAR with respect to the weighted monomial order with weight vector $\vec{c}=(1,3)$. Note, that the result $G_{<_{(1,3)}}=\{x^3-y, y^2-x^2y\}$ is not the same as the Gröbner basis with respect to lexicohraphic monomial order $G_{<_{lex(y>x)}}=\{-x^5+x^6, -x^3+y\}$.

```
                     SINGULAR                                 /
 A Computer Algebra System for Polynomial Computations       /   version 3-1-4
                                                           0<
 by: W. Decker, G.-M. Greuel, G. Pfister, H. Schoenemann     \   Jan 2012
FB Mathematik der Universitaet, D-67653 Kaiserslautern        \

 > ring r1=0, (x,y),Wp(1,3);
 // ** redefining r1 **
 > poly f1=-x3+y;
 > poly f2=x2*y-y2;
 > ideal I=f1,f2;
 > ideal gI=groebner(I);
 > gI;
 gI[1]=x3-y
 gI[2]=y2-x2y
```

Figure 5: *Gröbner basis $G_{<_{(1,3)}}$ of $\langle x^3-y, -x^2y+y^2\rangle$ computed in SINGULAR*

Recall that to solve a system of linear equations, an effective method is to reduce it to the form in which an initial string of variables is missing from some of the equations, that is, the so-called "row-echelon" form. The next definition and theorem provide a way to eliminate a group of variables from a system of nonlinear polynomials. Moreover, it provides a way to find all solutions of a polynomial system in the case that the solution set is finite, or in other words, to find the variety of a polynomial ideal in the case that the variety is zero-dimensional.

For any ideal $I=\langle f_1,\dots,f_s\rangle \subset k[x_1,x_2,\dots,x_n]$ the l −th elimination ideal I_l is the ideal of $k[x_{l+1},x_{l+2},\dots,x_n]$ defined by

$$I_l = \mathrm{I} \cap k[x_{l+1}, x_{l+2}, \dots, x_n].$$

In the case of solving a system of nonlinear equations (1.1), this means that $I = \langle f_1, \dots, f_s \rangle$, but the elements of I_l are the equations (polynomials) that follow from $f_1 = 0, \dots, f_s = 0$ and eliminate the variables $x_1, \dots, x_l$. Concerning the Gröbner bases and elimination ideals, we have the following

Theorem, ([4]). If $G = \{g_1, \dots, g_t\}$ is a Gröbner basis for $I = \langle f_1, \dots, f_s \rangle \subset k[x_1, \dots, x_n]$ with respect to lexicographic order with $x_1 > \cdots > x_n$, then for each $0 \leq l \leq n$ the set

$$G_l = \mathrm{G} \cap k[x_{l+1}, x_{l+2}, \dots, x_n]$$

is a Gröbner basis for the l −th *elimination ideal*.

Gröbner basis theory allows one to find all solutions of a system (1.1) if the system has only a finite number of solutions. In such case a Gröbner basis with respect to the lexicographic order is always in a “row-echelon” form, as can be seen using the following example, [5]. Consider the polynomials

$$f_1 = x^2 + yz + x$$
$$f_2 = z^2 + xy + z$$
$$f_3 = y^2 + xz + y.$$

With respect to the lexicographic order with $x > y > z$, the Gröbner basis of ideal $\langle f_1, f_2, f_3 \rangle$ is $G = \{g_1, g_2, g_3, g_4, g_5, g_6\}$, where

$$g_1 = x + x^2 + yz$$
$$g_2 = xy + z + z^2$$
$$g_3 = z + xz + yz + z^2 + 2yz^2$$
$$g_4 = y + y^2 - z - yz - z^2 - 2yz^2$$
$$g_5 = z^2 + 2yz^2 + z^3 + 2yz^3$$
$$g_6 = z^2 + 3z^3 + 2z^4.$$

Thus, the system $f_1 = f_2 = f_3 = 0$ is equivalent to the system

$$g_1 = g_2 = g_3 = g_4 = g_5 = g_6 = 0.$$

For a generic system (1.1), a Gröbner basis may have significantly more complex structure than obtained in this example. However, if the system has only a finite number of solutions (i.e. the ideal is zero-dimensional), then any reduced Gröbner basis $\{g_1, \dots, g_n\}$ must contain a polynomial in one variable, let say, $g_1(x_1)$. Then, there is a subset of the Gröbner basis depending on this variable and one more variable, say, $g_2(x_1, x_2), \dots, g_t(x_1, x_2)$, etc. Thus, we first solve (perhaps only numerically) the equation $g_1(x_1) = 0$. Then, for each solution x_1^* of $g_1(x_1) = 0$, we find the solutions of $g_2(x_1^*, x_2) = \cdots = g_t(x_1^*, x_2) = 0$, which is a system of

polynomials in a single variable x_2. Continuing the process, we obtain in this way all solutions to (1.1). Thus, in the case of the finite number of solutions, Gröbner basis computations theoretically provide the complete solution to the problem (see e.g. Section 2.2. of [1] for more details).

3 GRÖBNER BASIS AND INTEGER LINEAR PROGRAMMING

In previous sections, we considered the process of multi-division and the Gröbner bases theory. Before the formal definition of the integer linear programming problem, note that the essence of the problem concerns the integer solutions of a linear system $A\vec{x} = \overrightarrow{b}$ (constraints), which optimizes the so-called cost function. Therefore, it would be quite convenient if the rows of the matrix equation $A\vec{x} = \vec{b}$ (i.e. the equations) could be presented (in the first approximation) as exponents of some new variables. In order to make things more straightforward, let us consider $A\vec{x} = \vec{b}$ (where: $[A]_{i,j} = a_{i,j}$ and $\vec{b} = (b_1, \dots, b_m)$) with the following restrictions: $a_{i,j} \in \mathbb{Z}$, $b_i \in \mathbb{Z}$ and $c_j \in \mathbb{R}$ with $i = 1,2, \dots, n$ and $j = 1,2, \dots, m$. We want to find a solution $\vec{x} = (x_1, x_2, \dots, x_n) \in \mathbb{Z}^n$ to

$$\begin{aligned} a_{11}x_1 + a_{12}x_2 + \cdots + a_{1n}x_n &= b_1 \\ &\vdots \\ a_{m1}x_1 + a_{m2}x_2 + \cdots + a_{mn}x_n &= b_m, \end{aligned} \tag{3.1}$$

which minimizes the cost function $c(x_1, x_2, \dots, x_n) = \sum_{j=1}^{n} c_j x_j$. We call (3.1) an integer (linear) program (IP). In the matrix form, we have

$$\text{minimize } \vec{c} \cdot \overrightarrow{x}, \text{ subject to } A\vec{x} = \vec{b},$$

where $A \in \mathbb{Z}^{m\times n}$ *and* $\vec{b} = (b_1, \dots, b_m) \in \mathbb{Z}^m$. Note that all coefficients (including the solution vector) are generally allowed to be from the set $\mathbb{Z}$, but for now let the coefficients be limited to be natural numbers: $\mathbb{N}$.

The main mathematical idea which makes use of Gröbner bases when solving IP (3.1) is to associate new variables X_k for $k = 1,2, \dots, m$ (one variable to each equation) to (3.1) to represent the k −th equation in (3.1):

$$X_k^{a_{k1}x_1 + a_{k2}x_2 + \cdots + a_{kn}x_n} = X_k^{b_k} \leftarrow \mathrm{X_k} \text{ represents the } k - \text{th equaition}$$

The use of new variables makes the formulation of system (3.1) much simpler:

$$X_1^{a_{11}x_1 + a_{12}x_2 + \cdots + a_{1n}x_n} \cdots X_m^{a_{m1}x_1 + a_{m2}x_2 + \cdots + a_{mn}x_n} = X_1^{b_1} \cdots X_m^{b_m},$$

which is equivalent to

$$\left(X_1^{a_{11}} \cdots X_m^{a_{m1}}\right)^{x_1} \cdot \ldots \cdot \left(X_1^{a_{1n}} \cdots X_m^{a_{mn}}\right)^{x_n} = \vec{X}^{\vec{b}}. \tag{3.1a}$$

Note that in (3.1a) the original (integer) variables X_k $(k = 1, \dots, n)$ adopt the meaning of the (integer) exponent of $X_1^{a_{1k}} \cdots X_m^{a_{mk}}$. Therefore, to each column of (3.1) or equivalently to each term in the brackets $(\dots)$ in (3.1a), we associate a new variable $Y_k = X_1^{a_{1k}} \cdots X_m^{a_{mk}}$ for each $k = 1,2, \dots, n$.
The *first step* in solving our IP problem is to determine whether a solution exists or not. The theory of Gröbner bases helps to characterize the existence and finally to prove the *optimality of the solutions* to IP (3.1).
The *crucial idea in solving* (3.1) in terms of Gröbner bases plays the following ring homomorphism

$$\Phi: k[Y_1, \dots, Y_n] \to k[X_1, \dots, X_m],$$

which associates to any polynomial from the ring $k[Y_1, \dots, Y_n]$ a polynomial from the ring $k[X_1, \dots, X_m]$, which is defined by:

$$\Phi(Y_k) = X_1^{a_{1k}} \cdots X_m^{a_{mk}}. \tag{3.2}$$

We immediately see that homomorphism (3.2) is in a one-to-one relation with a system of the form (3.1) (more precisely, the image of every Y_k is bijective related with the k-th column on the left side of (3.1)); furthermore, according to (3.1a), we have

$$\Phi\left(Y_1^{x_1} \cdot \dots \cdot Y_n^{x_n}\right) = \vec{X}^{\vec{b}}.$$

Concerning the map Φ defined by (3.2) we can assert the following. If we assume that all coefficient $a_{i,j}$ and b_i from (3.1) are non-negative, then a solution $\vec{x} = \tilde{x} \in \mathbb{N}_0^n$ of (3.1) exists if and only if the monomial $X_1^{b_1} \cdots X_m^{b_m}$ is in the image under homomorphism Φ. This means that a monomial $\vec{Y}^{\tilde{x}} \in k[Y_1, \dots, Y_n]$ exists for which $\Phi(\vec{Y}^{\tilde{x}}) = X_1^{b_1} \cdots X_m^{b_m}$, and $\tilde{x} \in \mathbb{N}_0^n$ is a solution to (3.1).

Both implications of the above assertion can be proved at once. Let $\tilde{x} = (\tilde{x}_1, \tilde{x}_2, \dots, \tilde{x}_n) \in \mathbb{N}_0^n$ be a solution of (3.1). This means that (3.1a) holds for $\vec{b} = \tilde{x}$. According to definition of Φ this is equivalent to

$$(\Phi(Y_1))^{\tilde{x}_1} \cdots (\Phi(Y_n))^{\tilde{x}_n} = X_1^{b_1} \cdots X_m^{b_m}$$

Now, since Φ is a homomorphism we have

$$\Phi(Y_1^{\tilde{x}_1} \cdots Y_n^{\tilde{x}_n}) = X_1^{b_1} \cdots X_m^{b_m}$$

and $X_1^{b_1} \cdots X_m^{b_m}$ is in the image under Φ and the corresponding original is $Y_1^{\tilde{x}_1} \cdots Y_n^{\tilde{x}_n} \in k[Y_1, \ldots, Y_n]$, and we have shown that this is equivalent to $\tilde{x} = (\tilde{x}_1, \tilde{x}_2, \ldots, \tilde{x}_n) \in \mathbb{N}_0^n$ being solution to (3.1).

This means that $\tilde{x}$ for which $\vec{Y}^{\tilde{x}}$ is in the image under Φ is an integer solution to system (3.1), but still we have to handle the problem of the minimality condition of the cost function $c(x_1, x_2, \ldots, x_n) = \sum_{j=1}^n c_j x_j$. In order to solve this, we need some additional results. First, if $x_1, x_2, \ldots, x_n$ and $y_1, y_2, \ldots, y_n$ are elements of a commutative ring k, then for any non-negative integers $\alpha_1, \alpha_2, \ldots, \alpha_n$ the polynomial $x_1^{\alpha_1} x_2^{\alpha_2} \cdots x_n^{\alpha_n} - y_1^{\alpha_1} y_2^{\alpha_2} \cdots y_n^{\alpha_n}$ is in the ideal $\langle x_1 - y_1, \ldots, x_n - y_n \rangle$. The proof can be done by mathematical induction on the number of elements x_n and y_n. Let us simply mention that for $n = 1$ (the basis for induction) the assertion is a well-known result

$$x^\alpha - y^\alpha = (x - y)(x^{\alpha-1} + x^{\alpha-2}y + \cdots + xy^{\alpha-2} + y^{\alpha-1}).$$

For the rest of the proof, see [12].
Now let $K = \langle Y_1 - f_1, \ldots, Y_n - f_n \rangle \subseteq k[Y_1, \ldots, Y_n, X_1, \ldots, X_m]$ and $f_n \in k[X_1, \ldots, X_m]$. If $g \in K \cap k[Y_1, \ldots, Y_n]$, then $g(Y_1, \ldots, Y_n) = \sum_{i=1}^n (Y_i - f_n) h_i$, where $h_i \in k[Y_1, \ldots, Y_n, X_1, \ldots, X_m]$. Let Φ map $Y_i \longmapsto f_i$. Then $g(f_1, \ldots, f_n)$=0, thus $\Phi(g) = 0$. In contrast, let $\Phi(g) = 0$ and let $g = \sum_\alpha c_\alpha Y_1^{\alpha_1} Y_2^{\alpha_2} \cdots Y_n^{\alpha_n}$ (where finitely many $c_\alpha \neq 0$). Since $g(f_1, \ldots, f_n)$=0, we have

$$g = g - 0 = g - g(f_1, \ldots, f_n)$$

$$g = \sum_\alpha c_\alpha Y_1^{\alpha_1} Y_2^{\alpha_2} \cdots Y_n^{\alpha_n} - \sum_\alpha c_\alpha f_1^{\alpha_1} f_2^{\alpha_2} \cdots f_n^{\alpha_n}$$
$$g = \sum_\alpha c_\alpha \left(Y_1^{\alpha_1} Y_2^{\alpha_2} \cdots Y_n^{\alpha_n} - f_1^{\alpha_1} f_2^{\alpha_2} \cdots f_n^{\alpha_n} \right)$$

which is in the ideal $K = \langle Y_1 - f_1, \ldots, Y_n - f_n \rangle$, according to the previous result. Thus, $Ker(\Phi) = K \cap k[Y_1, \ldots, Y_n]$, and the elements of $Ker(\Phi)$ can (by the elimination theorem) be found in the following way: first find the Gröbner basis of the ideal $K = \langle Y_1 - f_1, \ldots, Y_n - f_n \rangle$ in $k[Y_1, \ldots, Y_n, X_1, \ldots, X_m]$ with respect to a lex ordering $X_1 > \cdots > X_m > Y_1 > \cdots > Y_n$. Then a Gröbner basis for $K \cap k[Y_1, \ldots, Y_n]$ will be precisely the polynomials of the Gröbner basis of K that do not have any X variables. Obviously, for a given homomorphism Φ, any monomial $f \in k[Y_1, \ldots, Y_n]$ is not in the image of Φ. Let us denote the Gröbner basis of $K = \langle Y_1 - f_1, \ldots, Y_n - f_n \rangle$ obtained by the elimination theorem by $\tilde{G}$. According to the above results, we have

$$f \in Ker(\Phi) \Leftrightarrow \exists h \in k[Y_1, \ldots, Y_n] \quad s.t. \quad f \xrightarrow{\tilde{G}} h,$$

which is then the key to the solution of IP (3.1) constrained by the cost function $c(x_1, x_2, \ldots, x_n) = \sum_{j=1}^n c_j x_j$. Finally note that, if take care that the monomial order which is used to compute the Gröbner basis, $\tilde{G}_{<_c}$, of the ideal $K = \langle Y_1 - f_1, \ldots, Y_n - f_n \rangle$ is compatibile with the cost function $c(x_1, x_2, \ldots, x_n) = \sum_{j=1}^n c_j x_j$ and with the corresponding

$$\Phi\left(Y_1^{x_1} \cdots Y_n^{x_n}\right) = \Phi\left(Y_1^{\tilde{x}_1} \cdots Y_n^{\tilde{x}_n}\right)$$

and

$$c(x_1, x_2, \ldots, x_n) < c(\tilde{x}_1, \tilde{x}_2, \ldots, \tilde{x}_n)$$

$$\Downarrow$$

$$Y_1^{x_1} \cdots Y_n^{x_n} <_c Y_1^{\tilde{x}_1} \cdots Y_n^{\tilde{x}_n}$$

then from $X_1^{b_1} \cdots X_m^{b_m} \xrightarrow{\tilde{G}_{<_c}} Y_1^{\tilde{x}_1} \cdots Y_n^{\tilde{x}_n}$ one can deduce that $\tilde{x} = (\tilde{x}_1, \tilde{x}_2, \ldots, \tilde{x}_n) \in \mathbb{N}_0^n$ is a solution to IP (3.1) for which the cost function $c(\vec{x}) = \vec{c} \cdot \vec{x}$ *is minimal.* The minimality of the solution is proven by contradiction. If any other solution $\vec{x} = (x_1, x_2, \ldots, x_n)$ is minimal then, since $c(\vec{x}) = c(\tilde{x})$ and since the term ordering $<_c$ is compatibile with the cost function and with the corresponding system we have $\Phi\left(Y_1^{x_1} \cdots Y_n^{x_n}\right) = \Phi\left(Y_1^{\tilde{x}_1} \cdots Y_n^{\tilde{x}_n}\right)$; implying $\Phi\left(Y_1^{x_1} \cdots Y_n^{x_n} - Y_1^{\tilde{x}_1} \cdots Y_n^{\tilde{x}_n}\right) = 0$, which means $Y_1^{x_1} \cdot\cdot Y_n^{x_n} - Y_1^{\tilde{x}_1} \cdots Y_n^{\tilde{x}_n} \xrightarrow{\tilde{G}_{<_c}} 0$, which contradicts the assumption that $Y_1^{x_1} \cdots Y_n^{x_n}$ is already reduced with respect to $\tilde{G}_{<_c}$.

The above results are the basis for Conti & Traverso's well-known algorithm, which is described below (see ([3]) for more details). However, first we have to consider how to transform (3.1) which can contain some negative integers; recall that generally $a_{i,j} \in \mathbb{Z}$ and $b_i \in \mathbb{Z}$. This can be generally transformed to an IP with strictly nonnegative (integer) coefficients $a_{i,j}, b_i$ by adding an extra indeterminate W defined by

$$X_1 \cdot X_2 \cdot \cdots \cdot X_m \cdot W = 1, \tag{3.3}$$

which transforms

$$\vec{X}^{Aj} := X_1^{a_{1j}} \cdot \ldots \cdot X_i^{-a_{ij}} \cdot \ldots \cdot X_m^{a_{mj}}$$

to

$$X_1^{a_{1j}+a_{ij}} \cdot \ldots \cdot X_i^{0} \cdot \ldots \cdot X_m^{a_{mj}+a_{ij}} \cdot W^{a_{ij}} = \vec{X}^{Aj} W_j,$$

where $W_j = W^{a_{ij}}$. In a similar way, if there are some negative entries in $\vec{b}$, we transform $\vec{X}^{\vec{b}}$ to $\vec{X}^{\vec{b}} W_{\vec{b}}$.

The optimal solution of IP (3.1) with some negative integers is, therefore, obtained in the following way:

- Define W by (3.3), if there are some negative entries in $A, \vec{b}$
- define an ideal $I = \left\{Y_1 - \vec{X}^{A_1}, \ldots, Y_n - \vec{X}^{A_n}\right\}$ on the polynomial ring $k[X_1, \ldots, X_m, Y_1, \ldots, Y_n]$, if there are no negative entries in $A, \vec{b}$

- define an ideal $I = \{Y_1 - \dot{X}^{A_1}W_1, \dots, Y_n - \dot{X}^{A_n}W_n, X_1 \cdot X_2 \cdot \dots \cdot X_m \cdot W - 1\}$ on the polynomial ring $k[X_1, \dots, X_m, W, Y_1, \dots, Y_n]$, if there are some negative entries in $A, \vec{b}$
- let G be a reduced Gröbner basisof $I$with respect to a monomial order $<_{\vec{c}}$, where $\vec{c}$ is defined by the cost function $\vec{c} \cdot \vec{x}$
- dividing $\vec{X}^{\vec{b}}W_{\vec{b}}$ (i.e. the generalization of $\vec{X}^{\vec{b}}$) by G always yields a remainder $R \in k[Y_1, \dots, Y_n]$, which because of its minimality (ensured by the multivariable division algorithm) ensures the optimality of the solution; thus the solution $\vec{x} = (\beta_1, \dots, \beta_n)$ to IP (3.1) is obtained by reducing $\vec{X}^{\vec{b}}W_{\vec{b}}$ by G which yields a remainder $R = {Y_1}^{\beta_1} \cdots {Y_n}^{\beta_n}$ and thereby the solution $\vec{x} = (\beta_1, \dots, \beta_n)$.

The next example will show the method for determining whether system of the form (3.1) has a non-negative integer solution, and for finding a solution. The method consists of the following three steps, [12]:

- Compute a Gröbner basis G for the ideal $K = \langle Y_j - X_1^{a_{1j}} \cdots X_m^{a_{mj}} : 1 \le j \le n \rangle$ with respect to an elimination order with the X variables greater than Y variables.
- Find the remainder r of the division of the monomial $X_1^{b_1} \cdots X_m^{b_m}$ by G.
- If $r \notin k[Y_1, \dots, Y_n]$, then system (3.1) does not have non-negative integer solutions. If $r = Y_1^{x_1} \cdots Y_n^{x_n}$, then $(x_1, \dots, x_n)$ is a solution of system (3.1), [1].

Now, we show how the proposed method works.

Example 1: Let us check if there exist non-integer solutions of system

$$2x_1 + x_2 = 3$$
$$x_1 + x_2 + 3x_3 = 5.$$

On the first step, we compute a Gröbner basis G of an ideal $K = \langle Y_1 - X_1^2X_2, Y_2 - X_{1X_2}, Y_3 - X_2^3 \rangle$ with respect to lexicographic order with $X_1 > X_2 > Y_1 > Y_2 > Y_3$. We obtain

$$G = \{-{Y_2}^6 + {Y_1}^3Y_3, X_2{Y_2}^4 - {Y_1}^2Y_3, X_2Y_1 - {Y_2}^2, {X_2}^2{Y_2}^2 - Y_1Y_3, {X_2}^3 - Y_3, -{X_2}^2Y_2 + X_1Y_3, -Y_1 + X_1Y_2, X_1X_2 - Y_2\}.$$

Then, we divide monomial $X_1^3X_2^5$ by G and obtain $Y_1^1Y_2^1Y_3^1$. Therefore, the non-negative integer solution is $(x_1, x_2, x_3) = (1,1,1)$.

Example 2 ([8]): We show how to optimize the cost function with respect to some constraints $A\vec{x} = \vec{b}$, and the coefficients are now allowed to be also negative integers. Following (3.1), we have to minimize the cost function

$$\vec{c} \cdot \vec{x} = 1000x_1 + x_2 + x_3 + 100x_4$$

subject to

$$3x_1 - 2x_2 + x_3 - x_4 = -1$$
$$4x_1 + x_2 - x_3 = 5.$$

The solution to the above example obtained with system SINGULAR is shown in Figure 6. Note that the weighted term order is used with $\vec{C} = (1000002,1000001,1000000,1000,1,1,100)$ to ensure that $X1 > X2 > W > Y1 > Y2 > Y3 > Y4$ and to ensure the weight order $(1000,1,1,100)$, corresponding to $\vec{c} = (1000,1,1,100)$. Note that, for example, the monomials $\vec{X}^{\vec{b}}W_{\vec{b}}$ and $\vec{X}^{A_2}W_2$ are:

$$\vec{X}^{\vec{b}}W_{\vec{b}} = X_1^{-1}X_2^5 = X_1^{-1}X_2^{-1} \cdot X_2^1X_2^5 = W^1X_2^6,$$
$$\vec{X}^{A_2}W_2 = X_1^{-2}X_2^1 = X_1^{-2}X_2^{-2} \cdot X_2^2X_2^1 = W^2X_2^3.$$

The optimal solution $\vec{x} = (1,3,2,0)$ is obtained from the result of the multivariable division:

$$W^1\ X_2^6 \xrightarrow{G} Y_1^1Y_2^3Y_3^2Y_4^0.$$

```
                     SINGULAR                                 /
 A Computer Algebra System for Polynomial Computations       /   version 3-
                                                            0<
 by: W. Decker, G.-M. Greuel, G. Pfister, H. Schoenemann     \   Jan 2012
FB Mathematik der Universitaet, D-67653 Kaiserslautern        \
> ring r1=0,(X1,X2,W,Y1,Y2,Y3,Y4),Wp(1000002,1000001,1000000,1000,1,1,100);
> poly f1=Y1-X13*X24;
> poly f1=Y1-X1^3*X2^4;
> poly f2=Y2-X2^3*W^2;
> poly f3=Y3-X1^2*W;
> poly f4=Y4-X2*W;
> poly f5=X1*X2*W-1;
> ideal I=f1,f2,f3,f4,f5;
> ideal gI=groebner(I);
> reduce(W*X2^6,gI);
Y1*Y2^3*Y3^2
>
```

Figure 6: *Computing the optimal solution in system SINGULAR*

References

[1] **W.W. Adams, P. Loustaunau:** An introduction to Gröbner bases: Graduate Studies in Mathematics. Vol. 3, Providence, RI: American Mathematical Society, 1994

[2] **B. Buchberger:** Ein Algorithmus zum Auffinden der Basiselemente des Restlasseringes nach einem nulldimensionalen Polynomideal. PhD Thesis, Mathematical Institute, University of Innsbruck, Austria, 1965

[3] **P. Conti, C. Traverso:** Buchberger algorithm and integer programming, Applied algebra, falgebraic algorithms and error-correcting codes (New Orleans, LA, 1991), Lecture Notes in Comput. Sci. vol. 539, p. 130-139, 1991

[4] **D. Cox, J. Little, D. O'Shea: I**deals, Varieties and Algorithms: An Introduction to Computational Algebraic Geomety and Commutative Algebra. New York: Springer, 2007

[5] **S.R. Czapor:** Gröbner basis methods for solving algebraic equations. Ph.D Thesis. University of Waterloo, Canada, 1988

[6] **V.F. Edneral, A. Mahdi, V.G. Romanovski, D.S. Shafer:** The center problem on a center manifold in R3, Nonlinear Anal., vol. 75, p. 2614-2622, 2012

[7] B. Ferčec, M. Mencinger: Isochronicity of centers at a center manifold, AIP conference proceedings, 1468. Melville, N.Y.: American Institute of Physics, p. 148-157, 2012

[8] **S. Flory, E. Michel:** Integer Programming with Gröbner basis. (http://www.iwr.uni-heidelberg.de/groups/amj/People/Eberhard.Michel/Documents/Else/DiscreteOptimization.pdf)

[9] **G.M. Greuel, G. Pfister, H. Schönemann:** Singular 3.0. A Computer Algebra System for Polynomial Computations, Centre for Computer Algebra, University of Kaiserslautern, 2005; http://www.singular.uni-kl.de.

[10] **V.G. Romanovski, M. Mencinger, B. Ferčec:** Investigation of center manifolds of 3-dim systems using computer algebra. Program. comput. softw., vol. 39, no. 2, p. 67-73, 2013

[11] **V.G. Romanovski, D.S. Shafer:** The center and cyclicity problems: A computational algebra approach. Boston: Birkhauser Verlag, 2009

[12] **C. Wendler:** Groebner Bases with an Application to Integer Programming; (http://documents.kenyon.edu/math/CWendler.pdf), 2004

JET Journal of Energy Technology

JET Volume 8 (2015) p.p. 59-70
Issue 2, October 2015
Typology of article 1.02
www.fe.um.si/en/jet.html

ELECTRIC CARS IN SLOVENIA

ELEKTRIČNI AVTOMOBILI V SLOVENIJI

Gregor Srpčič[ℜ]

Keywords: Electric vehicles, electric cars, charging stations, financial incentives

Abstract

This article deals with electric vehicles in Slovenia. The introduction of electric cars is necessary in order to achieve the objectives of the European Union's strategy for reducing CO_2 emissions from road vehicles. In the first part of the article, the development of electric cars and their functioning is described. A key component of electric cars are batteries; therefore, various types of batteries, battery charging, and types of charging stations, which occur in Slovenia, are described in this article. An extensive network of charging stations is essential for the use of electric vehicles. A map of charging stations and the number of charging stations in Slovenia are presented. Currently, the most charging stations are located in central Slovenia; this is in the area around Ljubljana. In addition, to an extensive network of charging stations, the introduction of electric vehicles also requires financial incentives to buyers of electric vehicles. Slovenian environmental public funds or Eco Fund grants provide financial incentives to buyers of electric cars. In Slovenia, there are two types of financial incentives.

Povzetek

Članek govori o električnih avtomobilih v Sloveniji. Uvajanje električnih avtomobilov je nujno za dosego ciljev strategije Evropske unije za zmanjšanje emisij CO_2 iz cestnih vozil. V prvem delu članka je opisan razvoj električnih avtomobilov in delovanje le-teh. Ključni sestavni del električnega avtomobila so baterije, zato so v članku opisani tudi različni tipi baterij, polnjenje baterij ter tipi polnilnih postaj, ki se pojavljajo v Sloveniji. Dobro razvejana mreža polnilnih postaj je nujna za uporabo električnih vozil. V članku je prikazan zemljevid in število polnilnih postaj v Sloveniji. Trenutno je največ polnilnih postaj lociranih v osrednji Sloveniji, torej v okolici Ljubljane. Poleg dobro razvejane mreže polnilnih postaj so pri uvajanju električnih vozil

[ℜ] Corresponding author: Gregor Srpčič, Tel.: +386 40 520 511, Mailing address: Faculty of energy technology, Hočevarjev trg 1, 8270 Krško, Slovenija

E-mail address: grega.srpcic@um.si

potrebne tudi finančne spodbude kupcem električnih vozil. V Sloveniji za finančne spodbude za nakup električnih vozil skrbi Slovenski okolijski javni sklad oziroma Eko sklad. V Sloveniji sta na voljo dva tipa finančnih vzpodbud.

1 INTRODUCTION

The European automotive industry is a world leader in developing clean and energy efficient technologies based on combustion engines, because it has invested heavily in research and development since the year 2000. It is also one of the key European industrial sectors, since it is competitive, innovative and supports a wide range of related industries, [1].

The European Union has set a long-term strategy to reduce CO_2 emissions from road vehicles and much has been realized already. Regulation (EC) No. 443/2009 on the setting emission performance standards for new cars requires that the target of reducing average CO_2 emissions of the new cars to 130 g/km be fully meet by 2015. The automotive industry will need to invest even more in emission abatement technologies, including intelligent traffic management technologies and further improve the efficiency of internal combustion engines, [1].

Providing long-term sustainable mobility calls for more energy-efficient vehicles that are powered by alternative energy sources. Electric vehicles offer a solution from the dependency on fossil fuels and for reducing CO_2 emissions. Electric vehicles are the first choice in transition to a more efficient traffic, [1].

2 DEVELOPMENT OF ELECTRIC VEHICLES

Electric vehicles embody our recent green-oriented mentality, but they are by no means a new innovation. They have been on the market for more than a century and have an interesting history of development, which continues. The first countries to develop an electric propulsion system were France and England. In 1835, Professor Sibrandus Stratingh drew a design of an electric car, which was later realized by his assistant Christopher Becker. In America, Thomas Davenport and Robert Davison, who made the electric vehicle more useful, contributed to the development of electric vehicles. In the following years, the development of electric vehicles went mainly towards the larger capacity of batteries for storing electricity, which was a prerequisite for a greater practicality of electric vehicles. Over the years, the highest possible speed of electric vehicles increased; in 1899, the limit of 100 km/h was broken. The speed achievement was credited to the Belgian Camille Jenatzy, whose vehicle was named ‘Never Satisfied’. Electric vehicles had, in comparison to other technologies in the industry, a number of advantages. Compared to vehicles powered by gasoline, they were quieter, did not spread any unpleasant odours in the surroundings and were not causing vibrations when functioning, [2], [3], [4].

A great advantage over petrol vehicles was also that there was no need to shift gears when driving, which was causing a lot of clumsiness in the competitive technology, [4].

The dominance of electric vehicles lasted somewhere until the beginning of the 1920s, with peak production in 1912, [3]. The reasons for the turnaround in the favour of the industry of vehicles with internal combustion engines are different. The construction of long roads between cities required a greater range of vehicles, which electric vehicles were not able to handle. In

Texas, new oil reserves were discovered, which reduced the cost of use of vehicles with internal combustion engines. The refinement of the ignition system of a petrol engine in 1912, which was presented by Charles Kettering, also had a significant impact on the turnaround. Ultimately the industry of petrol engines obtained its dominance with mass production of internal combustion cars from the Henry Ford factory, which offered vehicles to its customers that were more than half the price of electric cars, [2], [4].

Electric vehicles have been used only for specific purposes, such as vehicles for transporting milk, golf cars, and trucks. In the 1970s, the oil crisis has led to renewed interest in electric vehicles, which would alleviate the dependence of the transport sector on the situation on the oil market. The California Agency for Clean Air demanded that car manufacturers invest in the development of vehicles with low emission levels; the main objective were electric vehicles with zero emissions, [2], [5].

The biggest sales success was experienced by the EV1 model from General Motors, which represented the only car that met all the objectives of the Office for Energy of United States of America upon its arrival on the market. It was produced from 1996 to 2002 and was offered to customers through a lease agreement. As a reason for halting the production of the EV1, General Motors stated a lack of profitability. The public blamed pressure of oil lobbies and the fear of automobile companies about any strict rules regarding automotive emissions in other countries. Some of the EV1 autos are kept in various technical museums, but most were scrapped and recycled, although users of EV1 created strong publicity against these measures, [2], [5].

In 2004, the company Tesla Motors began developing an electric sports car, the Tesla Roadster, which came on the market in 2008. The Roadster was the first car with a built-in Li-ion battery. It boasts record-breaking driving performance, since it can travel 320 km on a single charge and accelerate from 0 to 100 km/h in just 4 s. [2], [5].

3 WHAT ACTUALLY IS AN ELECTRIC VEHICLE?

An electric vehicle is a vehicle that is powered solely by electricity stored in batteries located inside the vehicle. In a simple propulsion system, an accumulator powers an electric motor that enables the rotation of the wheels through mechanical transmission. This kind of a drive system reflects the simplicity of construction and good efficiency, [6]. An electric vehicle does not generate greenhouse gases. It can be powered by electricity generated from renewable energy sources; not only is the level of pollution zero, but the use of electricity generated from renewable energy sources also reduces the level of emissions, [2], [7].

Advantages of electric vehicles over conventional vehicles are lower maintenance costs, since the electric vehicle has fewer moving parts, thus allowing better utilization of energy. Electric vehicles do not need engine oil, a clutch or a transmission, and enable linear accelerations [7]. Due to the silent operation of the electric motor, it does not cause noise pollution and offers a more comfortable ride for passengers, [2].

Several types of electric vehicles are defined: battery electric vehicles, plug-in hybrids, and extended-range electric vehicles. A battery electric vehicle is a vehicle that uses only the energy stored in the batteries for propulsion. Plug-in hybrid vehicles use battery power as the main source for short distances, but at the same time, the internal combustion engine is running

when the batteries are depleted. Extended-range electric vehicles use battery power as the main source for short distances, but when the battery is depleted, an internal combustion engine, which provides power to the electric motor, begins to operate, [2], [8].

Ball et al. [8] also distinguish different classes or categories of electric vehicles. In the L6e category are four-wheelers with a maximum authorized carrying capacity of 550 kg together with batteries and a maximum output of 4 kW of the drive motor. Such vehicles are especially suitable for urban driving, [9]. They are allowed to be driven by persons over the age of fifteen years, pensioners and drivers without B and B1 driving license. In the L7e category of vehicles are four-wheelers with a maximum weight of 400 kg and a maximum specified drive motor power of 15 kW. In this category, the maximum prescribed vehicle weight of 400 kg is without batteries. Electric vehicles in this category meet the definition of an urban electric car and are well suited for driving in urban areas. In the M1 category of vehicles are four-wheeled passenger vehicles that are intended for the transport of up to eight passengers, together with the operator of the vehicle, [2], [9].

4 BATTERIES AND CHARGING OF BATTERIES

There are several types of batteries, whose most important characteristics are specific power, specific energy, charging efficiency, the number of charging cycles and, of course, price, [2], [10].

Lead acid batteries have the longest history of use; consequently, they have a well-developed recycling process, [10]. This type of battery is very affordable; they have high voltage galvanic cells and are still in use today. Their drawback is their weight, fast draining and the impossibility of refilling if they are empty for too long, [2].

The advantage of NiMH batteries is fast charging. Their weaknesses are high price and rapid self-discharge. The use of Ni-MH batteries in electric vehicles was most widespread at the turn of the century when they have replaced lead acid batteries in the well-known EV1 model of General Motors [2], [11].

A significant leap forward regarding capacity was made with the introduction of Li-Ion batteries. Their advantages are a highly adaptable design, small weight in comparison with the other types of batteries, a small percentage of self-discharge and no memory effect, [11]. One disadvantage of Li-Ion batteries is that they lose their original capacity over time, [2].

At present, Li-FePO4 batteries have the best characteristics. They are based on the technology of Li-Ion batteries, but they differ in the selected cathode material. Their advantages are stability and security, because when in use there is no possibility of overcharging or short-circuit shock. Physical damage to the battery cannot cause an explosion. They provide a high number of refilling cycles, they are resistant to high temperatures and allow discharges with high currents. Li-FePO4 batteries also allow rapid charging and are half the weight of lead acid batteries, [12].

Table 1: *Characteristics of batteries, [13]*

Type	Specific energy [Wh/kg]	Energy density [Wh/l]	Specific power [W/kg]	Charging efficiency [%]	Lifetime [cycles]
Pb	35-40	70	100-150	68	300-500
Ni-MH	50-60	175	200	76	600-1000
Li-Ion	80-90	200	<1000	80	1200
Li-FePO4	110	220	<3000	90	2000

Table 1 clearly shows that Li-FePO4 batteries have the best characteristics, they exceed other types of batteries in all characteristics that are given in Table 1.

Several different ways of charging electric cars exist. Typically, electric vehicles are recharged at home through a single-phase 220 V socket. Charging takes place via a power adapter that is already installed in the vehicle. This way of charging has a power supply of 3 kW and is usually very slow. For faster charging of electric vehicles, manufacturers of charging stations have developed a power adapter, of 22 or 43 kW, which is installed in the vehicle. Charging also takes place through three-phase socket outlets with a voltage of 400 V and the use of an external charger with an AC-DC converter. The charging power is 50 kW, [2], [14].

Table 2: *Technical characteristics of charging stations, [14]*

Charging time [h]	Power supply	Voltage	Maximum current
6-8	Single phase – 3.3 kW	220 VAC	16 A
2-3	Three-phase – 10 kW	400 VAC	16 A
3-4	Single phase – 7 kW	220 VAC	32 A
1-2	Three-phase – 24 kW	400 VAC	32 A
0.3-0.5	Three-phase – 43 kW	400 VAC	63 A
0.3-0.5	Direct current – 50 kW	400-500 VDC	100—125 A

Table 2 shows that the charging process takes the longest time at a voltage of 220 V, a maximum current of 16 A and a single-phase power supply with the power of 3.3 kW, which represents a home socket outlet. The battery of an electric vehicle is recharged in the shortest time with a DC power supply with power of 50 kW, voltage of 400 to 500 V and current of 100 to 125 A. [2], [14]

5 CHARGING STATIONS

Electric vehicles need charging stations, where batteries are filled with electric energy. In most cases, the manufacturer of electric vehicles or batteries provides a suitable charger, through which energy is transferred from the energy grid to the battery. The charging of electric vehicles is similar to charging the battery in a mobile phone; the only difference is that greater electrical power is needed for charging electric vehicles. Several alternative methods for charging electric vehicles are developed, including those that obtain energy from renewable energy sources, [2], [15].

The existing infrastructure of gas stations in developed countries makes it easy to introduce an additional offer of electric charging stations. On the existing electrical installation charging stations that enable the transmission of electricity into electric vehicles could be connected. In addition to petrol stations, it is reasonable to install fast charging stations in all areas with many parking spaces. These are, for example, public parking spaces and parking spaces of hotels, airports, restaurants, shopping centres, and similar facilities, as well as parking spaces used by employees of businesses during working hours, [2], [14].

Charging stations are roughly divided into two categories, which differ according to the use of the charger. A smart charging station is connected directly to the battery, which is recognized by the charging station itself. Other charging stations represent just a source of electrical power. There are two methods of charging: traditional or conductive connection and inductive connection, [2], [15].

In the case of conductive charging, the connector provides a secure connection between the charging station and the charging connector on the vehicle. The electric vehicle is connected to the primary outlet that usually has a voltage of 220 V at home; electric current flows from the charging station through the charging adapter into the battery and thus charges the battery of the electric vehicle. The charger is usually located outside the vehicle, or it may be installed in the vehicle. In the case of inductive charging, the charger has no direct electrical connection to the vehicle, as the energy is transmitted through a magnetic field, [15]. The identification of the user is of major importance for the application of charging stations. User identification allows charging for use, prohibition of use, activation or deactivation of the device. Several different methods of identification have been developed. The charging station can identify the user via a personal identification code (PIN), through radio frequency identification (RFID), over messages sent from a mobile phone or via a key belonging to a specific individual. [2], [16]

Borzen (Slovenian power market organizer) and SODO (electricity distribution system operator) are responsible for the infrastructure of charging stations for electric vehicles in Slovenia according to the proposal of the National Energy program (NEP), [2]. The most active companies in this area are electricity distribution companies Elektro Maribor and Elektro Ljubljana. The first

public charging station in Slovenia was activated on 9 April 2009 in Ljubljana, at Castle Kodeljevo, [2]. In summer 2015, the map of public charging stations in Slovenia (on the website of the company Elektro Ljubljana) lists 127 public charging stations; 58 of them are located in the vicinity of Ljubljana, and the fewest charging stations are in the northwest and southeast of Slovenia, [17].

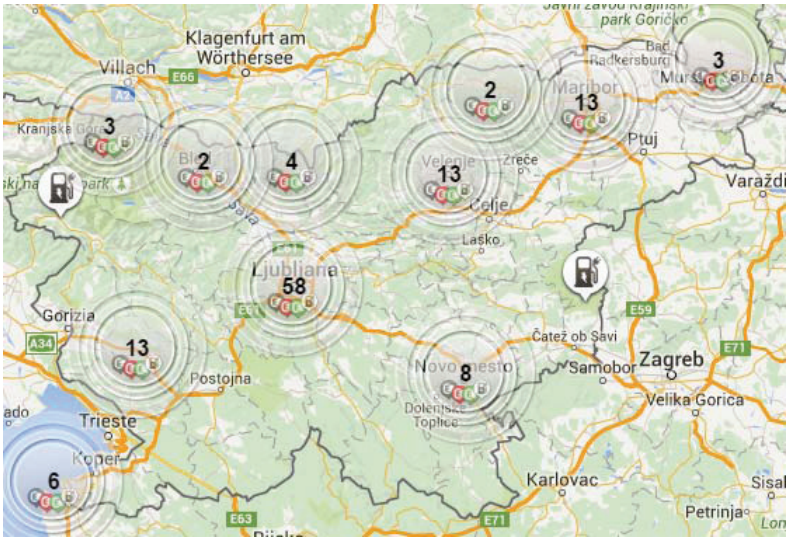

Figure 1: *Detailed map of charging stations in Slovenia (Source*: http://www.elektro-crpalke.si/*, 31.8.2015)*

Slovenia's largest provider of public charging stations is Elektro Ljubljana, which enables the charging of electric cars, electric motorcycles, and bicycles with an electric motor. Various charging stations have different ways of connection. Connecting via the infrared port (IR ID), activation by using users' mobile phone (GSM) or the charging station is activated, and the vehicle merely has to be connected (Plug & Charge), [18].

In public charging stations in Slovenia six types of connectors can be found (Figure 2): normal socket, 3-pin socket, 5-pin socket, 7-pin socket, CHAdeMO DC Quick charger and Tesla Supercharger. [17]

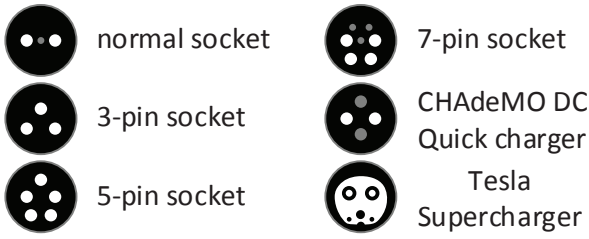

Figure 2: *Types of connectors, [17]*

Figure 3: *Etrel's charging station (Source:* http://polnjenjeev.etrel.si/grid/evcharging_we_our_solutions*, 31.8.2015)*

The charging station consists of a robust housing that resists unfavourable weather conditions, and the ergonomic design is easy to use. Charging the user for the service is ensured by using user identification and embedded counters. The charging station allows users to book a charging station, see the consumed energy and send messages to the users' mobile phone about the completion or an unexpected interruption of charging. For the users of electric vehicles, a web portal is also available. This web portal provides users with information about the occupancy of charging stations, with the ability to book a charging station and with the supervision of charging of users' electric vehicle. The portal also functions as a mobile application, through which the user searches for and books free charging stations and also supervises the recharging of his electric vehicle, [2], [19].

6 FINANCIAL INCENTIVES FOR THE PURCHASE OF ELECTRIC VEHICLES IN SLOVENIA

In Slovenia in 2015, there are currently two financial incentives for the purchase of electric vehicles.

6.1 Public tender 31SUB-EVOB15

Public tender 31SUB-EVOB15 concerns non-refundable financial incentives to individuals for purchase or investment into electric vehicles. An individual is eligible for a grant:

- in the case of purchasing a new electric vehicle,
- in the case of purchasing a new hybrid vehicle,
- in the case of purchasing a new electric vehicle with a range extender, or
- in the case of converting a vehicle with internal combustion engine into an electric vehicle, [20].

Grants may be awarded for the purchase of vehicles in categories L7e, L6e, N1 and M1 with electric propulsion without CO_2 emissions. Incentives can also be granted for the purchase of hybrid vehicles and vehicles with a range extender; however, CO_2 emissions must not exceed 50 g of CO_2 emissions per km, [20].

The total budget for the public tender is €500,000. The amount of the financial incentive is:

- €5,000 for a new or a processed electric vehicle without CO_2 emissions in the category M1;
- €3,000 for a new or a processed electric vehicle without CO_2 emissions in the category L7e;
- €3,000 for a new hybrid vehicle or an electric vehicle with a range extender with CO_2 emissions less than 50 g of CO2 emissions per km.
- €2,000 for a new or a processed electric vehicle without CO_2 emissions in the category L6e, [20].

Each natural person that has a permanent residence in Slovenia is entitled to the financial incentive, [20].

6.2 Public call for loans for environmental investments 53PO15

The subject of the public call is loans, for environmental investments, of the Eco Fund. Among the environmental investments are, [21]:

- Purchase of an electric vehicle with zero CO_2 emissions.
- Purchase of a hybrid vehicle or a vehicle with a range extender. CO_2 emissions of the mentioned vehicle types must not exceed 110 g/km, [21].

The total budget for the mentioned public tender is ten million euros. Loans are available for companies, entrepreneurs and natural persons with permanent residence in Slovenia. Loans are not available to legal entities that, [21]:

- do not have settled overdue financial obligations to the Slovenian Eco found;
- do not have settled tax or other financial obligations to the Republic of Slovenia;
- have a blocked bank account, [21].

The minimum amount of loan is €25,000, and the maximum amount is two million euros. The total debt of the borrower at the Eco Fund may not exceed ten million euros. The interest rate on the loan is EURIBOR plus a minimum of 1.5%. The repayment period is five years for the purpose of purchasing electric vehicles, [21].

7 CONCLUSION

In 2014, Slovenia had 1,412,315 registered road vehicles. Unfortunately, the Statistical Office of the Republic of Slovenia did not collect data about what powered them before 2014, and there is not yet any data for 2015. However, in 2014, around 53% of registered road vehicles were using gasoline, around 47% of registered road vehicles used diesel, and only 0.001% of all registered road vehicles were electric vehicles. In 2014, there were 153 registered electric vehicles and 86% of those were less powerful passenger cars, [22].

As already mentioned in Chapter 5, there are already 127 public charging stations in Slovenia. The network of charging stations in Slovenia is constantly expanding. Electric charging stations are and will be part of the Slovenian power grid; therefore, they represent a consumer of electrical energy. However, even in the case of a widespread use of electric vehicles and thus an extensive network of charging stations, the latter would not represent a significant load on the Slovenian network. If there were 500,000 electric cars in Slovenia and each of them would travel 20,000 km per year, with a consumption of 100 Wh/km, we would require an average power of 114 MW to charge all the electric cars. This represents only 5% of the total energy produced, [2], [15].

As said in Chapter 6, in Slovenia there are also financial incentives for the purchase of electric cars and thus long-term sustainable mobility. Electric vehicles will still cover the current target markets. A rapid increase in the use of electric vehicles is expected when battery technologies will improve. Studies show that the market for electric vehicles will comprise 1 to 2.7 % of the total market in 2020 and 11 to 30% of the total market in 2030, [1].

For hybrid cars, the expected sale is 4% in 2020 and 5 to 20% in 2030. For buyers of electric vehicles, the economic efficiency of vehicles is most important. The price of electric vehicles will have to decrease due to the progress in the electric vehicle technology and market demand. Electric vehicles have enormous potential for the solution to the challenges of the European Commission such as climate changes, independence from fossil fuels, local air quality, and the storage of renewable energy over the smart grid, [1].

References

[1] Informacija o trendih uveljavljanja baterijskih električnih vozil s predlogom ukrepa zagotavljanja infrastrukture, sistemskega okolja in vzpostavitve demonstracijskega projekta, Služba vlade Republike Slovenije za podnebne spremembe, http://www.vlada.si/fileadmin/dokumenti/Slikce/fotoarhiv/2010/SPS/_Informacija_o_trendih_uveljavljanja_baterijskih_elektri_350nih_vozil_.pdf (7th September 2015)

[2] **L. Juteršek:** Smiselnost nakupa električnega avtomobila, Fakulteta za logistiko, Univerza v Mariboru, Maribor, 2012.

[3] **M. Bellis:** History of electric vehicles, http://inventors.about.com/od/estartinventions/a/History-Of-Electric-Vehicles.htm (7th September 2015)

[4] **J. Aleksič:** Kratka zgodovina električnega vozila, http://www.mladina.si/45593/kratka_zgodovina_elektricnega_avtomobila/ (7th September 2015)

[5] History of electric vehicle, Wikipedia, https://en.wikipedia.org/wiki/History_of_the_electric_vehicle (7th September 2015)

[6] Zakon o dopolnitvah zakona o davku od dohodkov pravnih oseb – pojasnilo oziroma definicija hibridnega in električnega pogona vozila, Davčna uprava Republike Slovenije, http://www.durs.gov.si/si/davki_predpisi_in_pojasnila/davek_od_dohodkov_pravnih_oseb_pojasnila/davcne_olajsave/zakon_o_dopolnitvah_zakona_o_davku_od_dohodkov_pravnih_oseb_pojasnilo_oziroma_definicija_hibridnega_in_elektricnega_pogona_vozila/ (7th September 2015)

[7] E-mobilnost, Elektro Maribor, http://www.elektro-maribor.si/index.php/obnovljivi-viri/66-e-mobil (7th September 2015)

[8] **R. Ball, Na. Keers, M. Alexander, E. Bower:** Mobile energy resources in grids of electricity, http://www.transport-research.info/Upload/Documents/201402/20140203_154622_76425_Deliverable_2.1_Modelling_Electric_Storage_devices_for_Electric_Vehicles.pdf (7th September 2015)

[9] Program ukrepov za zagotavljanje infrastrukture in sistemskega okolja za vstop baterijskih električnih vozil na slovenski trg, Služba vlade Republike Slovenije za podnebne spremembe, http://www.arhiv.svps.gov.si/fileadmin/svps.gov.si/pageuploads/EBV_Program_ukrepov.pdf (7th September 2015)

[10] **G. Lampič:** Analiza uvajanja električnih pogonov v različne vrste vozil in zasnova pogona za sodobni mestni električni hibridni avto (SMEH), Fakulteta za elektrotehniko, Univerza v Ljubljani, Ljubljana, 2006.

[11] General motors EV1, Wikipedia, https://en.wikipedia.org/wiki/General_Motors_EV1 (7th September 2015)

[12] Tehnologija LiFePo4 akumulatorjev, e-avto.si, http://www.eavto.si/koristne-informacije/114-tehnologija-lifepo4-akumulatorjev (7th September 2015)

[13] **D. Motaln:** Konstrukcija in regulacija električnih vozil, Fakulteta za elektrotehniko, računalništvo in informatiko, Univerza v Mariboru, Maribor, 2009

[14] Charging station, Wikipedia, https://en.wikipedia.org/wiki/Charging_station (7th September 2015)

[15] Analiza optimalnih možnosti uvajanja sodobnega električnega osebnega prometa v slovenskih mestih, Elaephe, Ljubljana, 2008, http://in-wheel.com/media/website/test-library-slo/analizauvajanjaev_studijaelaphezamop.pdf (7th September 2015)

[16] E-Mobility 2013, Walther electro technical systems, http://www.waltherelectric.com/PDFs/emobility.pdf (7th September 2015)

[17] Slovenski iskalnik polnilnih mest za električna vozila, Elektro črpalke, http://www.elektro-crpalke.si/ (7th September 2015)

[18] Oprema polnilne postaje, Elektro črpalke, http://www.elektro-crpalke.si/1/Baza-znanja/Oprema-polnilne-postaje.aspx (7th September 2015)

[19] Web portal: Etrel elektromobilnost, http://www.etrel.si/ (7th September 2015)

[20] Javni poziv 31SUB-EVOB15, Eko sklad, Slovenski okoljski javni sklad, https://www.ekosklad.si/dokumenti/rd/31SUB-EVOB15/1__31SUB-EVOB15_Javni_poziv.pdf, (15th September 2015)

[21] Javni poziv za kreditiranje okoljskih naložb 53PO14, Eko sklad, Slovenski okoljski javni sklad, https://www.ekosklad.si/cms/tinymce/upload/53PO15/0__Javni%20poziv%2053PO15.pdf, (16th September 2015)

[22] After two years of decline, the number of registered passenger cars in 2014 up again, Statistical office of Republic of Slovenia, http://www.stat.si/StatWeb/en/show-news?id=5227&idp=22&headerbar=21

Journal of Energy Technology

Author instructions

www.fe.um.si/en/jet.html

MAIN TITLE OF THE PAPER
SLOVENIAN TITLE

Author[1], Author [2], Corresponding author[R]

Keywords: (Up to 10 keywords)

Abstract

Abstract should be up to 500 words long, with no pictures, photos, equations, tables, only text.

Povzetek

(Abstract in Slovenian language)

Submission of Manuscripts: All manuscripts must be submitted in English by e-mail to the editorial office at jet@um.si to ensure fast processing. Instructions for authors are also available online at http://www.fe.um.si/en/jet/author-instructions.html.

Preparation of manuscripts: Manuscripts must be typed in English in prescribed journal form (MS Word editor). A MS Word template is available at the Journal Home page.

A title page consists of the main title in the English and Slovenian language; the author(s) name(s) as well as the address, affiliation, E-mail address, telephone and fax numbers of author(s). Corresponding author must be indicated.

Main title: should be centred and written with capital letters (ARIAL bold 18 pt), in first paragraph in English language, in second paragraph in Slovenian language.

Key words: A list of 3 up to 6 key words is essential for indexing purposes. (CALIBRI 10pt)

Abstract: Abstract should be up to 500 words long, with no pictures, photos, equations, tables, - text only.

Povzetek: - Abstract in Slovenian language.

[R] Corresponding author: Title, Name and Surname, Tel.: +XXX x xxx xxx, Mailing address: xxxxxxxxxxxxxxxxxxxxxx xxxxxxxxxx, E-mail address: x.x@xxx.xx

[1] Organisation, Department, Address

[2] Organisation, Department, Address

[3] Organisation, Department, Address

Main text should be structured logically in chapters, sections and sub-sections. Type of letters is Calibri, 10pt, full justified.

Units and abbreviations: Required are SI units. Abbreviations must be given in text when first mentioned.

Proofreading: The proof will be send by e-mail to the corresponding author in MS Word's Track changes function. Corresponding author is required to make their proof corrections with accepting or rejecting the tracked changes in document and answer all open comments of proof reader. The corresponding author is responsible to introduce corrections of data in the paper. The Editors are not responsible for damage or loss of submitted text. Contributors are advised to keep copies of their texts, illustrations and all other materials.

The statements, opinions and data contained in this publication are solely those of the individual authors and not of the publisher and the Editors. Neither the publisher nor the Editors can accept any legal responsibility for errors that could appear during the process.

Copyright: Submissions of a publication article implies transfer of the copyright from the author(s) to the publisher upon acceptance of the paper. Accepted papers become the permanent property of "Journal of Energy Technology". All articles published in this journal are protected by copyright, which covers the exclusive rights to reproduce and distribute the article as well as all translation rights. No material can be published without written permission of the publisher.

Chapter examples:

1 MAIN CHAPTER

(Arial bold, 12pt, after paragraph 6pt space)

1.1 Section

(Arial bold, 11pt, after paragraph 6pt space)

1.1.1 Sub-section

(Arial bold, 10pt, after paragraph 6pt space)

Example of Equation (lined 2 cm from left margin, equation number in normal brackets (section. equation number), lined right margin, paragraph space 6pt before in after line):

Equation (1.1)

Tables should have a legend that includes the title of the table at the top of the table. Each table should be cited in the text.

Table legend example:

Table 1: *Name of the table (centred, on top of the table)*

Figures and images should be labelled sequentially numbered (Arabic numbers) and cited in the text – Fig.1 or Figure 1. The legend should be below the image, picture, photo or drawing.

Figure legend example:

Figure 1: *Name of the figure (centred, on bottom of figure, photo, or drawing)*

References

[1] **N. Surname:** Title, Publisher or Journal Title, Vol., Iss., p.p., Year of Publication

Examples:

[2] **J. Usenik:** Mathematical model of the power supply system control, Journal of Energy Technology, Vol. 2, Iss. 3, p.p. 29 – 46, 2009

[3] **J.J. DiStefano, A.R. Stubberud, I.J.Williams:** Theory and Problems of Feedback and Control Systems, McGraw-Hill Book Company, 1987

Example of reference-1 citation: In text [1], text continue.

Nomenclature

(Symbols)	(Symbol meaning)
t	time

JET

ISSN 1855-5748

JET | Journal of Energy Technology | Vol.1, Issue 2, October 2015 | University of Maribor, Faculty of Energy Technology